BMC Genomics

RESEARCH

Open Access

Comprehensive analysis of the *INDETERMINATE DOMAIN* (*IDD*) gene family in *Marchantia polymorpha* brings new insight into evolutionary developmental biology

Congye Zhou[1], Ting Yang[1], Manlei Cai[1], Hongchang Cui[2], Fei Yu[1], Huawei Liu[1] and Jing Fu[1*]

Abstract

Background SHORTROOT (SHR) and SCARECROW (SCR) are key regulators of plant cell fate. An increasing number of studies have illustrated that the SHR-SCR pathway depends on some INDETERMINATE DOMAIN (IDD) family transcription factors in regulating genes involved in tissue and organ morphogenesis, nutrients transport and metabolism, photoperiodic flowering and stress response. Recent genome sequencing and analysis revealed that only seven *IDD*s exist in the liverwort *Marchantia polymorpha*, one of the early diverging extant land plant lineages. However, little is known concerning how the IDDs and the SHR/SCR-IDD pathway work in the ancestral land plants.

Results In this study, *IDD* gene family members of this liverwort and other classic model plants were classified into seven branches on the basis of phylogenetic analysis. Gene structure and protein motif analyses suggested that most of the Mp*IDD*s are comparatively evolutionary conserved. Protein structure prediction showed that MpIDDs display similar core domain organization with the IDD proteins from the same branches. *Cis*-regulatory element prediction demonstrated that Mp*IDDs* might be hormone and stress responsive. The expression levels of most Mp*IDD*s display tissue specificities and could be changed by hormone treatment. All the MpIDDs are located in the nucleus, and most of them have autoactivation activity. Yeast two-hybrid assays confirmed the interactions between MpGRAS8/MpSHR and MpIDD3, MpIDD4 or MpIDD5, as well as MpGRAS3/MpSCR and MpIDD1 or MpIDD2. Taken together, our results provide comprehensive information on *IDD* gene family in *M. polymorpha* for further exploring their function in depth, and highlight the importance of the SHR/SCR-IDD pathway in plant development and evolution.

Conclusions Through bioinformatics analysis and experimental determination of expression patterns, subcellular localization, autoactivation, and protein interaction, this study provided crucial information for a deeper understanding of the functions of MpIDDs in evolutionary developmental studies.

Keywords *Marchantia polymorpha*, *INDETERMINATE DOMAIN* gene family, Phylogenetic analysis, Protein motifs prediction, Expression pattern, Protein–protein interactions

*Correspondence:
Jing Fu
jingfu@nwafu.edu.cn
Full list of author information is available at the end of the article

Introduction

Plant development process is controlled elaborately by transcription factors (TFs). TFs are expressed in specific stages and tissues, and bind to the promoters of downstream genes for transcriptional regulation independently or cooperatively by recruiting other TFs, to determine the destiny of plant tissues and cells thereby. The classic SHORTROOT (SHR)-SCARECROW (SCR) pathway plays pivotal roles in plant development [1–5]. An increasing body of evidence has demonstrated that the *INDETERMINATE DOMAIN* (*IDD*) family genes are expressed in a tissue and cell type-specific manner, and regulate plant development through forming complex with SHR-SCR [6–11].

SHR and SCR, members of the plant specific GRAS (GIBBERELLIC ACID INSENSITIVE, REPRESSOR OF GA1, and SCARECROW) transcription factor family, are critical for the cell fate determination and cell division/differentiation processes during plant development [1–5]. The expression pattern of *SHR* and *SCR* has an intimate relevance to their functions. In *Arabidopsis* root apical meristem, *SCR* is expressed in the quiescent center (QC), cortex-endodermis initial/daughter (CEI/CEID) and endodermis; The *SHR* transcript is made in the stele, but the SHR protein moves outwards to the cell layer where *SCR* is expressed. After entering the CEI/CEID, SHR activates the transcription of *SCR* and, along with SCR and other TFs, promote the transcription of cell cycle genes that are required for the periclinal division of CEID to form the endodermis and cortex [6, 9, 10, 12, 13]. The SHR-SCR complex hinders the further movement of SHR from the endodermis by increasing the transcription of *SCR*, ensuring the formation of a single layer of endodermis in plants. Therefore, SHR and SCR are both critical factors for the determination of the endodermal cell fate [6, 7, 9, 14, 15]. In QC cells, SCR functions upstream of the *RETINOBLASTOMA-RELATED* gene to control the expression of some cell cycle TFs for QC maintenance [16]. In *Arabidopsis* leaves, *SCR* is expressed in the bundle sheath cells, whereas *SHR* is expressed in the central xylem but the SHR protein moves to the outer bundle sheath cells [4, 17]. Mutations in *SHR* and *SCR* result in the loss or enlargement of the bundle sheath cells respectively [4]. Similarly, the transcription of *SCR* is also restricted in the starch sheath of hypocotyls or inflorescence stems [5, 18], and *SHR* is mainly transcribed in the vasculature of hypocotyls but the SHR protein moves to the adjacent starch sheath layer [5]. Both genes contribute to the gravitropic response and amyloplast sedimentation in hypocotyls [5, 19].

The IDD family belongs to a plant-specific transcription factor family characterized by the presence of multiple zinc finger motifs [20]. The diverse functions of the IDD family genes in the regulation of growth and development, hormone signaling and metabolic processes in angiosperms have been reviewed by Coelho et al. [21]. A series of researchers have associated the SHR-SCR pathway with IDD family members. Through transcriptional data mining and ChIP-PCR confirmation, two members of *IDD* family, *MAGPIE* (*MGP*) and *NUTC RACKER* (*NUC*) have been shown to be the direct targets of SHR and SCR in vivo [6, 7]. *JACKDAW* (*JKD*), another member of the *IDD* family, expresses mainly in the QC, the CEI/CEID and the ground tissue. *MGP* has similar expression pattern as *JKD*, but is excluded from the QC. *SHR* and *SCR* are both indispensable for the expression of *JKD* and *MGP*. Mutation in *JKD* causes slight reduction in root length and meristem cell number, disorganization of the QC, ectopic periclinal divisions in the cortex, and an increase in cortex and endodermis cell numbers. *JKD* acts mainly through SHR but not SCR in these processes. However, *MGP* has an opposite effect on the ground tissue patterning. Yeast two-hybrid and BiFC assays showed that JKD and MGP can interact with the SHR-SCR complex, and that SCR and JKD retain SHR in the nuclei of the QC and endodermis [8]. *BALDIBIS* (*BIB*), the closest homolog of *JKD*, shows a similar expression pattern to that of *JKD*. After the expression of *BIB* was knocked down in *jkd* background, an increase in both cell layers and cell number per layer was seen in the root meristem of the resulting plants. Although there are more cell layers, only one layer in the vicinity of the epidermis possesses endodermal identity. The additional ground tissue layers carry cortex identity. The epidermal cell fate also changes. These reprogrammed cell fates correlate with the ectopic activation of *CYCD6* expression in *jkd* and *jkd bib*. JKD, BIB and SCR on their own can individually bind SHR, but all together, they exhibit the strongest effect on SHR nuclear retention. The decreased BIB and JKD binding in *jkd bib* leads to expansion of the SHR protein expression domain [9]. More members of *IDD* family, *NUC*, *BLUEJAY* (*BLJ*) and *IMPERIALEAGLE* (*IME*), have been shown to be expressed in the ground tissue. Together with *SCR*, most of these ground tissue-specific *IDD* genes collaboratively maintain the ground tissue identity [10]. In rice, a monocot model plant, Os*SHR1*, Os*SHR2*, Os*IDD12* and Os*IDD13*, are all expressed in the vascular tissue of developing leaves [11]. The OsIDD12 and OsIDD13 dimer targets a *cis*-element in intron 3 of Os*PIN-FORMED (PIN) 5c*. The interaction of OsSHR1/2 with the OsIDD12/13 dimer mediates Os*PIN5c* repression. This SHR-IDD-PIN regulatory circuit modulates minor vein formation and ground cell differentiation [11]. In addition to the above evidence from molecular genetics, a crystal structure

of SHR-SCR-IDD10 (JKD) ternary complex has been resolved, which provides details concerning this canonical interaction [22].

IDD gene members have been identified in the genomes of *Arabidopsis* (16), rice (15) and maize (23) [20, 23, 24]. Functional characterization of *IDD* genes in these angiosperms are laborious and challenging, as some of the *idd* single mutants displayed no obvious or faint phenotype, and the phenotype was enhanced only when more related *IDD* members were mutated [9, 25–28]. With an important phylogenetic position, a low redundancy in regulatory genes and the feasibility of genetic transformation, the liverwort *Marchantia polymorpha* L. has become a new model plant for evolutionary developmental (evo-devo) studies [29, 30]. The *M. polymorpha* genome possesses only seven *IDD* family members, nearly one third of the numbers in model angiosperms [29]. The simple genomic context of *M. polymorpha* should facilitate the elucidation of the functions of Mp*IDD* genes. Furthermore, in order to adapt to the land, *M. polymorpha* has acquired a considerable number of new traits and regulatory strategies, which has been gradually refined during the evolution of modern plants. Thus, learning from *M. polymorpha* could shed light on numerous mechanisms that plants have adopted in the evolutionary courses.

However, to date, the functions of most Mp*IDD* genes have not been well-studied. The basic information concerning Mp*IDD* family genes is still uncharacterized. The interactions between MpIDDs and MpSHR or MpSCR have not been resolved. In the present study, we first undertook a phylogenetic analysis of *IDD* genes in representative plants from charophyte, liverwort, moss, lycophyte, gymnosperm and angiosperm. The Mp*IDD* gene structures, conserved protein motifs, protein structures and promoter elements were analyzed by bioinformatic tools. Tissue-specific expression and responses to phytohormones of Mp*IDDs* were then investigated by quantitative real-time PCR. The subcellular localization and autoactivation activity of MpIDDs were identified. Using yeast two-hybrid assay, the interactions between MpIDDs and SHR or SCR counterparts in the liverwort were determined. Together, these results provide the foundation for further functional dissection of Mp*IDDs* and help us understand the significance of the SHR/SCR-IDD pathway during the terrestrialization of plants.

Materials and methods

Datasets and sequence retrieval

All the protein amino acid sequences of *Klebsormidium nitens*, *Chara braunii*, *Anthoceros agrestis*, *M. polymorpha*, *M. polymorpha montivagans*, *Takakia lepidozioides*, *Physcomitrium patens*, *Selaginella moellendorffii*, *Picea abies*, *Arabidopsis thaliana*, *Oryza sativa* and *Zea mays* were obtained from http://www.plantmorphogenesis.bio.titech.ac.jp/~algae_genome_project/klebsormidium/kf_download.htm, https://plants.ensembl.org/Chara_braunii/Info/Index, https://www.hornworts.uzh.ch/en/hornwort-genomes.html, https://marchantia.info/, https://www.takakia.com/, Phytozome (https://phytozome-next.jgi.doe.gov/—genomic database versions: *Marchantia polymorpha* v6.1, *Physcomitrium patens* v6.1, *Selaginella moellendorffii* v1.0, *Pabies* 01, *Arabidopsis thaliana* TAIR10, *Oryza sativa* v7.0, and *Zea mays* RefGen_V4) [31] and PlantTFDB v.4.0 [32], and their previous identifiers were listed in Table S1. The Mp*IDD* 3.0 kb upstream promoter sequences and gene information were acquired from Phytozome. The protein sequences and MpIDDs DNA sequences files in FASTA format were in supplementary materials.

Plant materials and treatments

The plant used in this study was *M. polymorpha* accession Takaragaike-1 (Tak-1) donated by professor Chizuko Yamamuro from Fujian Agriculture and Forestry University Haixia Institute of Science and Technology. Thalli were cultivated on half-strength Gamborg's B5 (1/2B5) medium plus 1% sucrose and 1% Agar under 16-h light/8-h dark cycle at 22℃.

For tissue-specific expression analysis, the samples were collected from meristem, gemma cup, gemma, rhizoid and whole sample of the three-week-old Tak-1 plants. For hormone treatments, 10-day-old gemmae grown on 1/2B5 medium were transferred to media containing 5 μM gibberellin (GA_3), 100 μM abscisic acid (ABA), 150 μM jasmonic acid methyl ester (MeJA), 1 μM indole-3-acetic acid (IAA), 0.1 mM salicylic acid (SA) or 50 μM 6-benzylaminopurine (6-BA) for 24 h, respectively. After hormone treatment, the whole samples were harvested. All the samples prepared with three biological replicates were frozen in liquid nitrogen immediately and stored in -80 ℃ for RNA isolation.

The IDDs phylogenetic analysis

To determine the evolutionary relationship between IDD proteins from representative plants of different species, two KnIDDs, two CbIDDs, four AaIDDs, seven MpIDDs, 9 MpmIDDs, six TlIDDs, 17 PpIDDs, 11 SmIDDs, 17 PaIDDs, 22 AtIDDs, 28 OsIDDs and 37 ZmIDDs were identified. The ClustalW v2.1 software [33] was used to conduct the multiple sequence alignments with default gap penalties. These sequence alignments were then manually adjusted to minimize insertion/deletion events to improve the reliability of the phylogenetic tree. Then MEGA version 11 [34] was used to construct a neighbor joining tree with the following parameters: No. of differences method, 10% site coverage cutoff, uniform rates

among sites and 1000 interior-branch tests. The phylogenetic tree file in Newick format has been provided in the supplementary materials.

Mp*IDD* gene structures analysis and conserved motifs prediction

For Mp*IDD* gene structures and conserved motifs analysis, the IBS version 1.0.3 software [35] was used to visualize genes exon–intron structures including exons, introns, UTRs and gene length. The online MEME suite 5.5.5 program (http://meme-suite.org) [36] was used to identify protein sequences for conserved motifs prediction with the following parameters: the maximum number of motifs, 4; the minimum motif width, 6; the maximum motif width, 50; the minimum sites per motif, 2; the maximum sites per motif, 6; and default parameters. Finally, motifs with low e-value were shown and used for analysis.

Protein 3D structure analysis

The IDD amino acid sequences were used to predict 3D structures for all MpIDDs and related AtIDDs or other IDDs from the same branch. 3D modeling was performed using the AlphaFold Server AlphaFold 3 (https://golgi.sandbox.google.com/) [37]. The result of the 3D structure prediction was visualized by PyMOL 3.1.3.1 [38].

Mp*IDDs cis*-regulatory elements prediction

To predict Mp*IDDs cis*-regulatory elements, putative *cis*-acting elements in 3.0 kb upstream promoter sequences of Mp*IDDs* were determined using the PlantCARE transcription factor 5.0 database (http://bioinformatics.psb.ugent.be/webtools/plantcare/html/) [39]. Finally, the types and numbers of predicted *cis*-acting elements of the Mp*IDD* genes were visualized by TBtools v2.034 [40].

RNA isolation and quantitative real-time PCR (qRT-PCR)

Total RNA was extracted using the RNAIso plus kit (TaKaRa Bio, Dalian, China). Genomic DNA was removed from total RNA using RNase-free DNaseI (Fermentas, USA). cDNA was obtained by PrimeScriptTM II 1st Strand cDNA Synthesis Kit (TaKaRa, Dalian, China). The expression level of each *MpIDD*s was monitored on a Biorad CFX Connect Real-Time PCR Detection System (BioRad, SG) using the ChamQ™ Universal SYBR qPCR Master Mix (Vazyme, Nanjing, China). Melting curve analysis showed that all the products generated single peaks. PCR primers were designed using Primer Premier 5.0 software and primer sequences were listed in Table S2. Internal control gene for qRT-PCR was Mp*EF1α* and its primer sequences was listed in Table S2. Each cDNA sample was quantified in technical triplicate and biological triplicate. The relative RNA level of each gene was calculated according to the $2^{-\Delta\Delta CT}$ method. Finally, the relative expression levels of Mp*IDD*s were visualized by GraphPad Prism version 8.0.2.263 for Windows.

Subcellular localization of MpIDD proteins

The coding sequences of Mp*IDD*s were amplified by PCR and cloned in-frame with the reporter gene *GFP* driven by 35S promoter. All the PCR primers for cloning were listed in Table S2. After verified by sequencing, the recombinants were transformed into *Agrobacterium tumefaciens* strain GV3101. The agrobacteria colonies were inoculated into the liquid Luria Broth (LB) and cultured at 28 ℃, 180 rpm for 36 h. The cells were pelleted by centrifugation and then dispersed in AS buffer (10 mM MES, 10 mM $MgCl_2$, 200 μM acetosyringone, pH5.7) to reach OD 0.6–0.8 at 600 nm. The resuspension was injected into the leaves of 4-week-old tobacco. After growing for 48 h at room temperature, the leaf epidermis cells were observed under light or fluorescence using Olympus BX53 compound microscope.

Autoactivation activity analysis of MpIDDs

The coding sequences of Mp*IDD*s were amplified from Tak-1 cDNA by PCR. The products were digested by relevant restriction enzymes and inserted into the pGBKT7 vector. All the PCR primers for cloning were listed in Table S2. The correct recombinants confirmed by sequencing were transformed into yeast strain AH109 and selected on SD:/-Trp medium (Solid medium without tryptophan). The successfully transformed yeast cells were grown on SD:/-Trp,-His medium (Solid medium without tryptophan and histidine) or SD-Trp-His plus X-α-gal media to test the autoactivation activities of MpIDDs.

The GRAS family phylogenetic analysis

To verify the evolutionary relationship of the *GRAS* family proteins in *Arabidopsis* and *M. polymorpha*, the ClustalW v2.1 program [33] was used to initially align *GRAS* family protein sequences with default gap penalties. These alignments were then adjusted to minimize insertion/deletion events manually. Finally, the MEGA version 11 program [34] was used to conduct the phylogenetic tree using the neighbor-joining method based on the No. of differences model with the following option settings: partial deletion for gaps, uniform rates among sites, 20% site coverage cutoff, 1000 interior-branch test and branches bootstrap values more than 50% were shown.

Yeast two-hybrid assay

Yeast two-hybrid was performed to determine the interactions between MpIDDs and MpGRAS8/MpSHR or MpGRAS3/MpSCR. The coding sequences of Mp*IDDs* were obtained by PCR and purified. The products were cut by restriction enzymes and inserted into the prey vector pGADT7 with the matching ends. The coding sequences of Mp*GRAS8*/Mp*SHR* and Mp*GRAS3*/Mp*SCR* were amplified and cloned into the bait vector pGBKT7 by ligation and In-Fusion Cloning, respectively. All the recombined vectors were verified to be correctly constructed by sequencing. The yeast cells co-transformed by the bait and prey vectors were grown on SD:/-Leu,-Trp medium (Solid medium without leucine and tryptophan) to select the successfully transformed clones containing both vectors. The protein interactions were confirmed by growing cells on SD:/-Leu,-Trp,-His,-Ade (Solid medium without leucine, tryptophan, histidine and adenine) or SD:/-Leu,-Trp,-His,-Ade, plus X-α-gal media. 40 mM of 3-aminotriazole (3-AT) was supplemented to the medium to suppress the autoactivation activities of MpGRAS8/MpSHR and MpGRAS3/MpSCR. All the PCR primers for cloning were listed in Table S2.

Results

The IDD family protein phylogenetic analysis

To explore the evolutionary relationship of IDDs, a phylogenetic tree was constructed with 162 IDD proteins from *K. nitens, C. braunii, A. agrestis, M. polymorpha, M. polymorpha montivagans, T. lepidozioides, P. patens, S. moellendorffii, P. abies, A. thaliana, O. sativa and Z. mays*, using neighbor-joining method followed by alignments of their full-length protein sequences (Fig. 1). These proteins were separated into seven branches (I, II, III, IV, V, VI and VII). Except for branch II, seven MpIDDs were grouped to the remaining six branches. In charophyte alga *K. nitens* and *C. braunii*, the common ancestors of the land plants [41, 42], only two IDD proteins were found respectively, which may be sister to all IDDs in land plants. IDDs in bryophyte groups, one hornwort (*A. agrestis*), two liverworts (*M. polymorpha* and *M. polymorpha montivagans*) and two mosses (*T. lepidozioides* and *P. patens*), were in close proximity to each other in most cases. It was as expected that most MpIDDs and MpmIDDs had the closest homology. Branch I had representatives from ten out of twelve chosen species. Thirteen *P. patens* IDDs with high homology were grouped together in branch I, as a consequence of whole genome duplication in moss [43]. MpIDD3 showed a close relationship with AtIDD3 and AtIDD8 in this branch. Branch II included a large number of IDD members from angiosperms, accounting for 17.3% of the total. We speculate that sequences clustered in branch II might function exclusively in angiosperms. Branch III owned MpIDD7, which showed homology to ZmID1 and OsID1. Branch IV contained nine species. MpIDD2 and the AtIDD14-16 subclade were grouped close to each other in branch IV. MpIDD3, MpIDD7 and MpIDD2 might perform conserved functions as AtIDDs, OsIDDs and ZmIDDs, as they were in the same branch. MpIDD4, MpIDD5 and 33 IDD proteins from other species were grouped in branch V, the functions of these proteins were largely unknown. MpIDD6 and most AtWIPs were the main members in branch VI. WIP domain containing proteins, named after their initial three amino acids, have a highly conserved C-terminal region consisting of four zinc fingers [44]. The WIP lineage could be considered as sister to the IDD lineage concerning the origin of IDD before flowering plants [45]. In branch VII, there were only three PaIDDs and three bryophyte IDDs, indicating that these IDDs might have functions different from those previously characterized in *Arabidopsis*, rice and maize.

Gene structure and motif composition of MpIDDs

The Mp*IDDs* gene sequences and structures were analyzed. The results showed that Mp*IDD1*, Mp*IDD4* and Mp*IDD5* are all single-exon genes of similar length, suggesting that they might have the same evolutionary origin and perform similar functions in *M. polymorpha*. Mp*IDD6* has two short exons that might be originated from an insertion event in a long exon. Mp*IDD7* is constituted by four short exons and its coding sequence is the shortest one. While Mp*IDD2* and Mp*IDD3* possess four and three exons, respectively, the total length of their exons is nearly the same, and both encode long proteins in *M. polymorpha* (Fig. 2A).

The IDD family proteins in angiosperms are characterized by the presence of a conserved ID domain, which consists of two C2H2 and two C2HC zinc-finger motifs with DNA-binding ability [20, 46, 47]. We found four types of conserved motifs in MpIDDs, among which only motif 1 is the standard C2H2 zinc finger, while motif 2 and 3 possess Cys/His-rich regions (CH3 in motif 2 and HC2 in motif 3) (Fig. 2B, Fig. S1). It has been reported that the CH3 motif could fold into a zinc finger and bind DNA properly [48]. Motif 4 seems to be an imperfect zinc finger motif with only a single residue of histidine and cysteine (Fig. S1). MpIDD1 to 7 have all four types of motifs (Fig. 2B).

SHR binding motif (RR/KDxxITHxAFCD), which is believed to constitute the interface between SHR and AtIDD10/JKD, is conserved in most *Arabidopsis* IDD protein members (AtIDD1-13) [22]. In *M. polymorpha* IDD proteins, only MpIDD3 possesses this motif (RRDSFITHRAFCD, residues 306–318), implying that MpIDD3 has the potential to form a heterodimer with MpSHR.

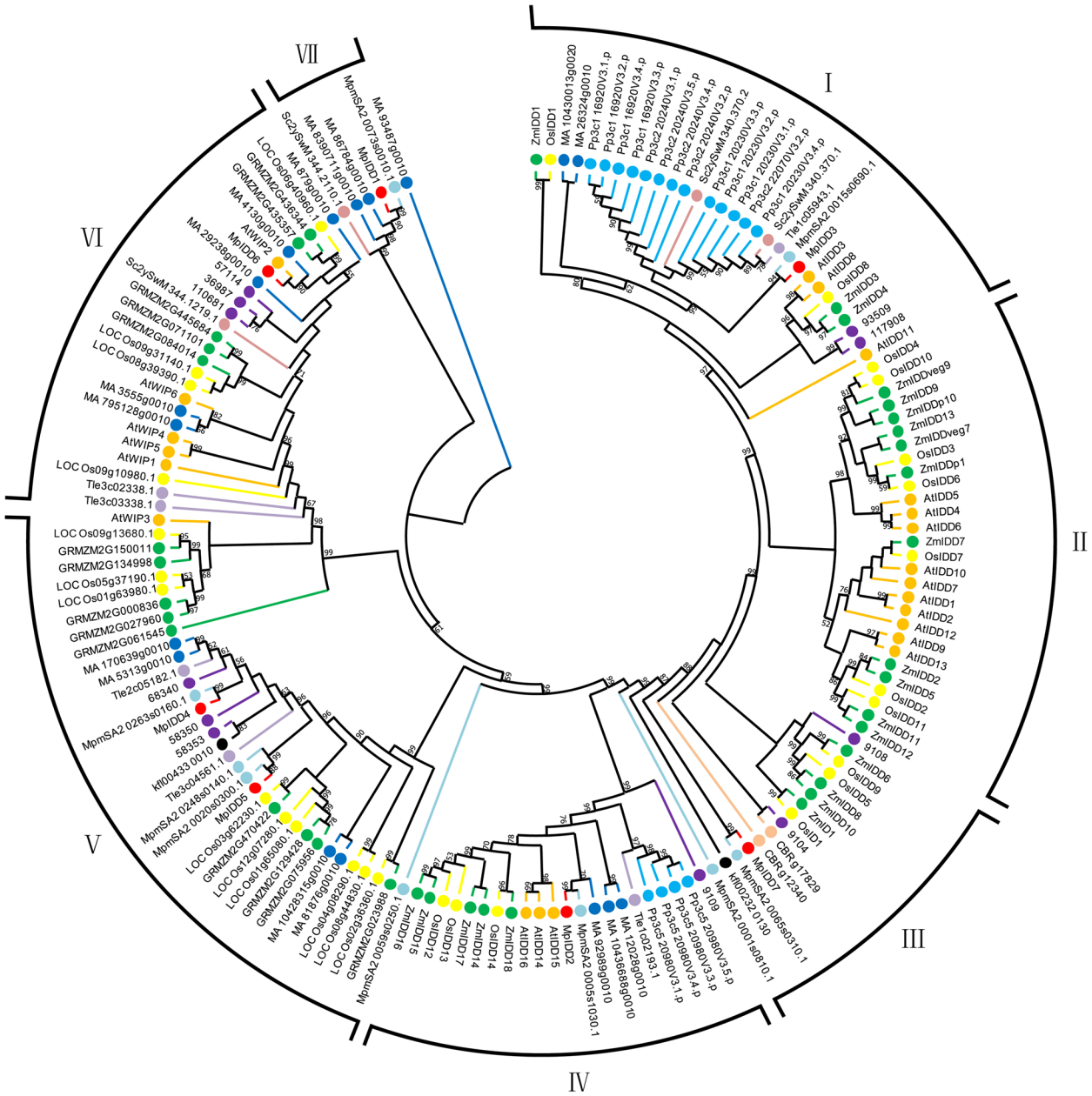

Fig. 1 Circular phylogenetic tree showing evolutionary relationships between KnIDD, CbIDD, AaIDD, MpIDD, MpmIDD, TlIDD, PpIDD, SmIDD, PaIDD, AtIDD, OsIDD and ZmIDD proteins. The evolutionary history was inferred by using the neighbor-joining method based on the No. of differences method with the following option settings: 10% site coverage cutoff, uniform rates among sites and 1000 interior-branch tests. The analysis involved 162 amino acid sequences. The IDD family protein sequences were obtained from http://www.plantmorphogenesis.bio.titech.ac.jp/~algae_genome_project/klebsormidium/kf_download.htm, https://plants.ensembl.org/Chara_braunii/Info/Index, https://www.hornworts.uzh.ch/en/hornwort-genomes.html, https://marchantia.info/, https://www.takakia.com/, Phytozome (genomic database versions: *Marchantia polymorpha* v6.1, *Physcomitrium patens* v6.1, *Selaginella moellendorffii* v1.0, *Pabies* 01, *Arabidopsis thaliana* TAIR10, *Oryza sativa* v7.0, and *Zea mays* RefGen_V4) [31] and PlantTFDB v.4.0 [32], and the ClustalW v2.1 software [33] was used to conduct the multiple IDD protein sequences alignments. The MEGA version 11 [34] was used to perform the evolutionary analyses. The accession numbers for these genes were listed in Supplementary Table S1. Black, incarnadine, grey orange, red, grey blue, light purple, blue, purple, indigo, orange, yellow and green represented IDD genes from *K. nitens*, *C. braunii*, *A. agrestis*, *M. polymorpha*, *M. polymorpha montivagans*, *T. lepidozioides*, *P. patens*, *S. moellendorffii*, *P. abies*, *A. thaliana*, *O. sativa* and *Z. mays*, respectively

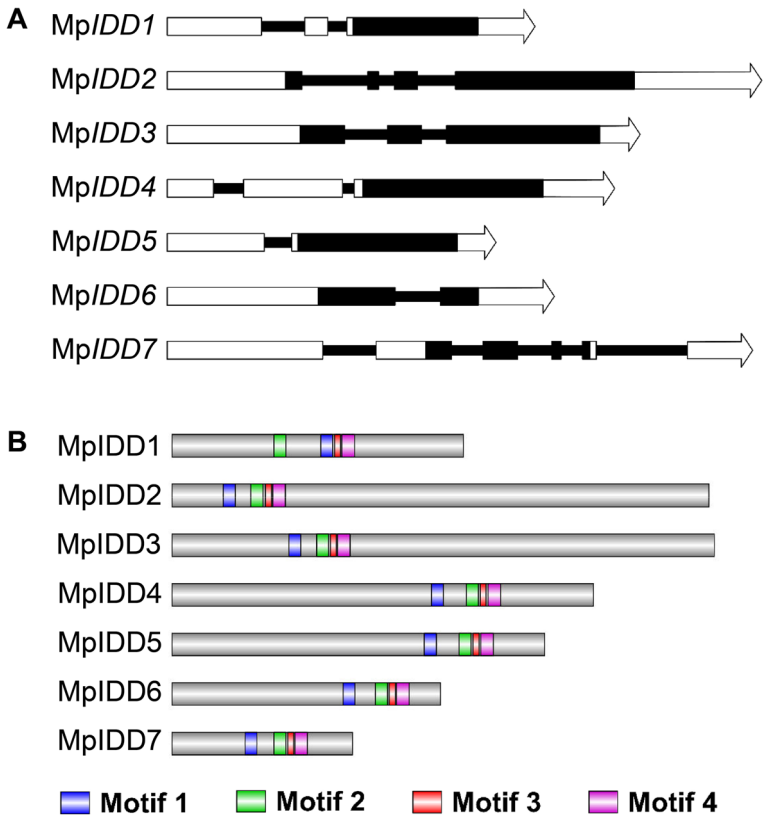

Fig. 2 Gene structures and conserved motifs in Mp*IDD* gene family. **A** Gene structures of Mp*IDD* family members were generated by IBS version 1.0.3 software [35]. The black boxes and arrows represented exons, and lines represented introns, while the white boxes and arrows indicated 5'-UTR and 3'-UTR, respectively. **B** Conserved motifs of MpIDD proteins. The online MEME suite 5.5.5 program (http://meme-suite.org) was used to identify conserved motif sequences. Different colored boxes represented different motifs. Motifs consensus sequences were displayed in Fig. S1

The 3D protein structure prediction of MpIDDs and related IDDs from other plant species

To gain further insights into the evolutionary relationship and potential functions of IDD proteins, the predicted 3D structures of the MpIDDs and related IDDs from the same branch were compared. The result revealed that these IDD proteins mainly consist of α-helices, β-sheets and random coils (Table 1). The MpIDDs exhibit main domains comprising Zinc Fingers (Fig. 3), in line with the preliminary secondary structure predictions (Table 1). The reliability scores of the core domain predictions were all above 50 (Fig. S2). In branch VII, MpIDD1 and an adjacent MpmIDD protein (MpmSA2 0073s0010.1) shared similar configuration (Fig. 3A). MpIDD2 and AtIDD14-16 were grouped in branch IV (Fig. 1), with the Zinc finger domains of MpIDD2 and AtIDD15 being nearly the same, and all owned a long α-helix at their C-termini (Table 1, Fig. 3B). In branch I, MpIDD3 showed homology to AtIDD3 and AtIDD8 (Fig. 1), and the arrangement of Zinc Finger domains of MpIDD3 and AtIDD3 was quite comparable to each other (Fig. 3C). In branch V, the Zinc Finger domains of MpIDD4 and MpIDD5 and their neighboring MpmIDD protein MpmSA2 0263s0160.1 and MpmSA2 0020s0300.1 had analogous structures (Fig. 3D and E). In branch VI, the Zinc Finger domains of MpIDD6 and AtWIP2 from the same clade almost overlapped (Fig. 3F). The organization of MpIDD7 and ZmID1 in branch III matched each other (Fig. 3G). The similarity residing in these IDD proteins implies that they might have shared functions and common evolutionary origins.

Cis-regulatory elements in MpIDDs

To gain insight into the functions of Mp*IDD*s, *cis*-regulatory elements in their promoter sequences, which were taken as 3.0-kb fragments upstream of the coding regions, were analyzed. The result showed that 29 types of *cis*-regulatory elements were present (Fig. 4, Table S3), which could be divided into three types: hormone response related elements, development-related elements, and abiotic stress related elements.

GA responsive element, ABA responsive element, MeJA responsive element, auxin responsive element and SA responsive element were classified into hormone

Table 1 The predicted secondary structures of IDD proteins in Fig. 3

Gene Name	Protein Full Length (aa)	α-helix (%)	β-sheet (%)	Random coil (%)
Mp*IDD1*	485	20.62	4.33	70.05
Mp*IDD2*	893	29.12	3.14	67.75
Mp*IDD3*	902	14.41	2.44	83.15
Mp*IDD4*	701	26.68	3.28	70.04
Mp*IDD5*	620	26.19	3.49	68.73
Mp*IDD6*	447	20.13	4.70	75.17
Mp*IDD7*	301	23.67	10.00	66.33
MpmSA2 0073s0010.1	490	15.51	4.49	80.00
AtIDD15	446	34.08	6.50	59.42
AtIDD3	506	19.96	5.73	74.31
MpmSA2 0263s0160.1	703	24.61	3.56	71.83
MpmSA2 0020s0300.1	707	32.81	3.11	64.07
AtWIP2	383	22.98	5.48	71.54
ZmID1	436	18.35	6.42	75.23

response related elements. Four out of seven Mp*IDD* genes own SA responsive element. ABA responsive element, auxin responsive element and MeJA responsive element were distributed in the promoters of all seven Mp*IDD*s, indicating that Mp*IDD*s might be involved in diverse hormone signaling pathways (Fig. 4, Table S3).

Meristem expression related element and light responsive element were grouped into development-related elements. In particular, six out of seven Mp*IDD* genes had meristem expression related elements and each Mp*IDD* possessed at least 11 light responsive elements, implying that Mp*IDD*s in *M. polymorpha* might participate in photosynthetic processes and mediate meristem morphogenesis (Fig. 4, Table S3).

Anoxic specific inducibility related element, anaerobic induction related element, low-temperature responsive element (LTR), defense and stress responsive element were grouped as abiotic stress related elements. Anoxic specific inducibility related element was distributed in all seven Mp*IDD*s. Four Mp*IDD*s harbored anaerobic induction related element, six Mp*IDD*s had LTR, and four Mp*IDD*s had defense and stress responsive element. These results suggested that Mp*IDD*s might be involved in stress-related biological processes in *M. polymorpha* (Fig. 4, Table S3).

Tissue-specific expression patterns of MpIDDs

To determine if Mp*IDD*s are involved in vegetative growth in a tissue-specific manner, we examined their expression patterns in different tissues of three-week-old *M. polymorpha* plants (Fig. 5, Fig. S3). The qRT-PCR results showed that, among the seven Mp*IDD* genes, Mp*IDD1* had the highest level of expression in the meristem, which suggests that Mp*IDD1* might influence plant growth processes. Mp*IDD2* expression was specific to gemma cups, indicating that this gene may play an important role in gemma cup development. Mp*IDD3* did not show an obvious expression preference in the meristem, gemma cups, gemmae or rhizoids, but displayed a slightly higher level of expression in the whole plant, suggesting the existence of more Mp*IDD3* transcript in the remaining parts of the thallus. The expression levels of Mp*IDD5* in rhizoids was extremely high, nearly four times that of the whole sample, revealing that Mp*IDD5* might be involved in rhizoid development. Contrary to Mp*IDD5*, Mp*IDD6* had a very low expression in rhizoids; instead, it was highly expressed in gemmae and meristem, showing that Mp*IDD6* might play a part in gemmae and meristem development. The transcript of Mp*IDD7* largely accumulated in gemma cups and meristem, implying a possible role of Mp*IDD7* in gemma cups and meristem

(See figure on next page.)

Fig. 3 The predicted 3D protein structure models of MpIDD proteins and structure alignment of MpIDDs and other IDDs from the same groups. The first column showed the 3D structures of MpIDDs, the second column showed the 3D structures of related IDD proteins from the same branches, the third column showed the structure alignments of MpIDD and related IDD proteins. In the first and second columns, α-helices, β-sheets and random coils were represented by dark green, yellow and gray respectively, and the gray balls denoted zinc atoms. In the third column, the 3D structures of MpIDDs and related IDDs were denoted as green and red respectively

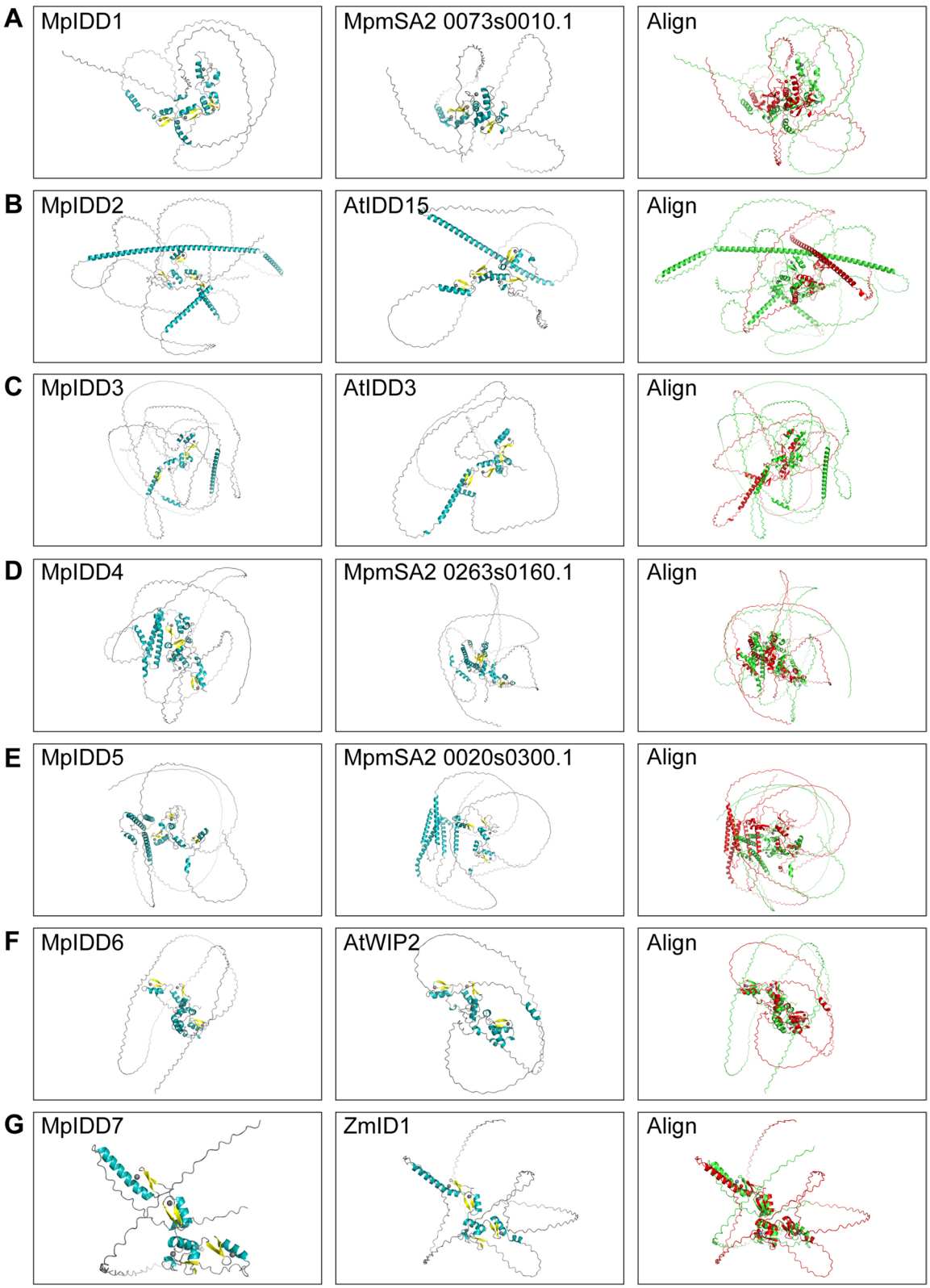

Fig. 3 (See legend on previous page.)

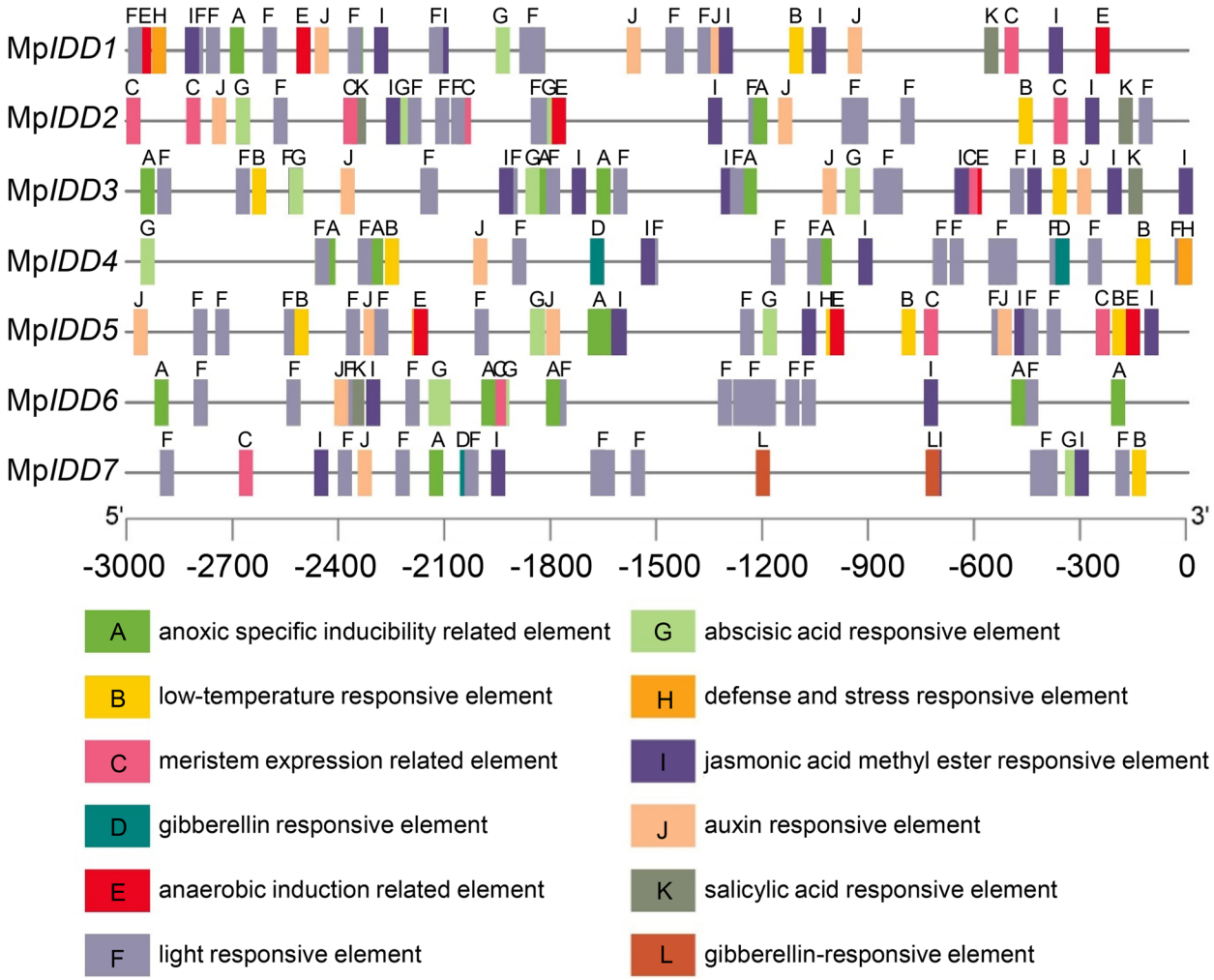

Fig. 4 Types and locations of predicted *cis*-regulatory elements of the Mp*IDD* genes. Elements were visualized using TBtools software. 3.0 kb upstream promoter sequences of Mp*IDD* genes were analyzed. Anoxic specific inducibility related element represented by GC-motif. Low-temperature responsive element, Meristem expression related element and Anaerobic induction related element were represented by LTR, CAT-box and ARE, respectively. Gibberellin responsive elements included TATC-box, P-box and GARE-motif. Light responsive element included GT1-motif, TCT-motif, Box 4, AE-box, Sp1, G-Box, I-box, ACE, ATCT-motif, GATA-motif, GATT-motif, TCCC-motif, GTGGC-motif, chs-CMA2a and AAAC-motif. ABA responsive element, Defense and stress responsive element and Salicylic acid responsive element were represented by ABRE, TC-rich repeats and TCA-element, respectively. MeJA responsive element included CGTCA-motif and TGACG-motif. Auxin responsive element included TGA-element and AuxRR-core. The information for all the *cis*-regulatory elements of the Mp*IDD* genes were listed in Table S3

development. Compared to other Mp*IDD*s, Mp*IDD4* had the least degree of tissue-specificity.

Responses of MpIDDs to phytohormone treatments

Based on the former *cis*-regulatory elements analysis results, we examined the responsiveness of Mp*IDDs* to hormone treatments through qRT-PCR. Six plant hormones (GA_3, ABA, MeJA, IAA, SA and 6-BA) were used (Fig. 6, Fig. S4). The results showed that none of the seven Mp*IDD*s respond to GA_3 at a concentration of 5 μM. ABA treatment obviously down-regulated the expression level of Mp*IDD1*, Mp*IDD2* and Mp*IDD5*. MeJA treatment caused an increase in the transcription level of Mp*IDD6* and Mp*IDD7*. IAA treatment suppressed the expression of Mp*IDD1*, but enhanced the expression of Mp*IDD2*, Mp*IDD3*, Mp*IDD6* and Mp*IDD7*. With SA treatment, the transcription level of Mp*IDD2*, Mp*IDD3* and Mp*IDD7* was elevated. Mp*IDD1* and Mp*IDD7* behaved oppositely in response to 6-BA treatment.

The subcellular localization and autoactivation activity of MpIDDs

After being translated in cytoplasm, TFs are transported into nucleus to regulate the expression of downstream

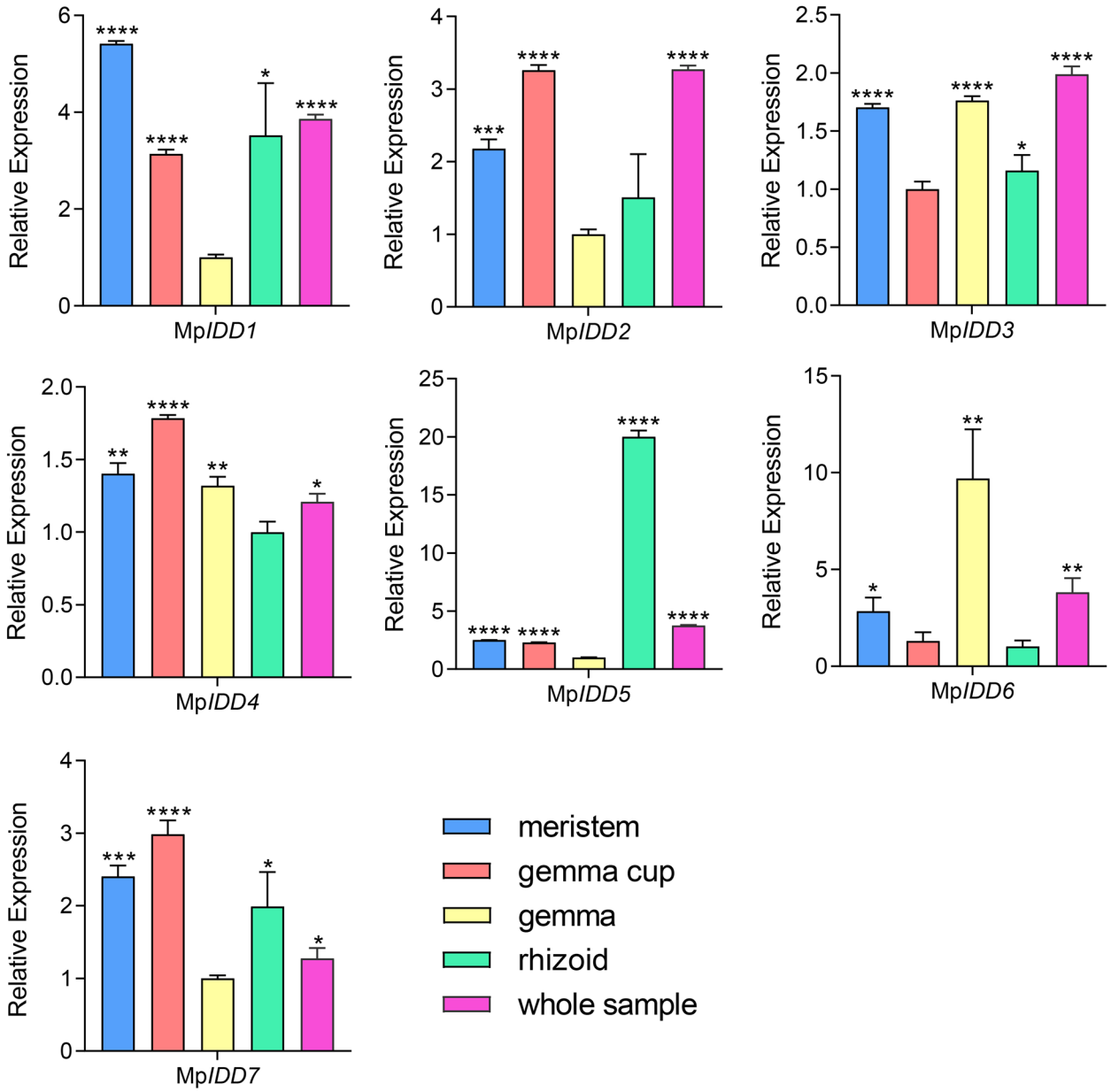

Fig. 5 The expression level of Mp*IDD1* to *7* in different tissues of three-week-old *M. polymorpha*. The bars are means ± standard deviation (SD) from three technical replicates. Three biological replicates and three technical replicates were conducted. All the experiments showed the same expression trend. Only one biological replicate was presented here, the other two replicates were included in Fig. S3. Mp*EF1a* was used as an internal control and the lowest expression level was set to 1. *t*- tests, * $P < 0.05$; ** $P < 0.01$; *** $P < 0.001$; **** $P < 0.0001$

genes. In order to determine if MpIDDs are TFs, we expressed their fusion proteins with Green Fluorescent Protein (GFP) in tobacco leaves using the *CaMV35S* promoter and examined their subcellular localization. The transient expressed fluorescence signals reflected the localization of MpIDDs. The signals of all seven MpIDD-GFP fusion proteins were observed mainly in the nucleus (Fig. 7), whereas the signal from the control, *CaMV35S*-driven GFP, was detected in both the nucleus and cytoplasm (Fig. 7). The nuclear localization of MpIDDs indicates that they might serve as TFs.

TFs bind to the promoters of downstream targets, activating or suppressing transcription. To investigate the transcriptional activity of MpIDDs, the coding sequences of Mp*IDD*s were fused with the GAL4 DNA binding domain in the pGBKT7 vector. The recombinants were

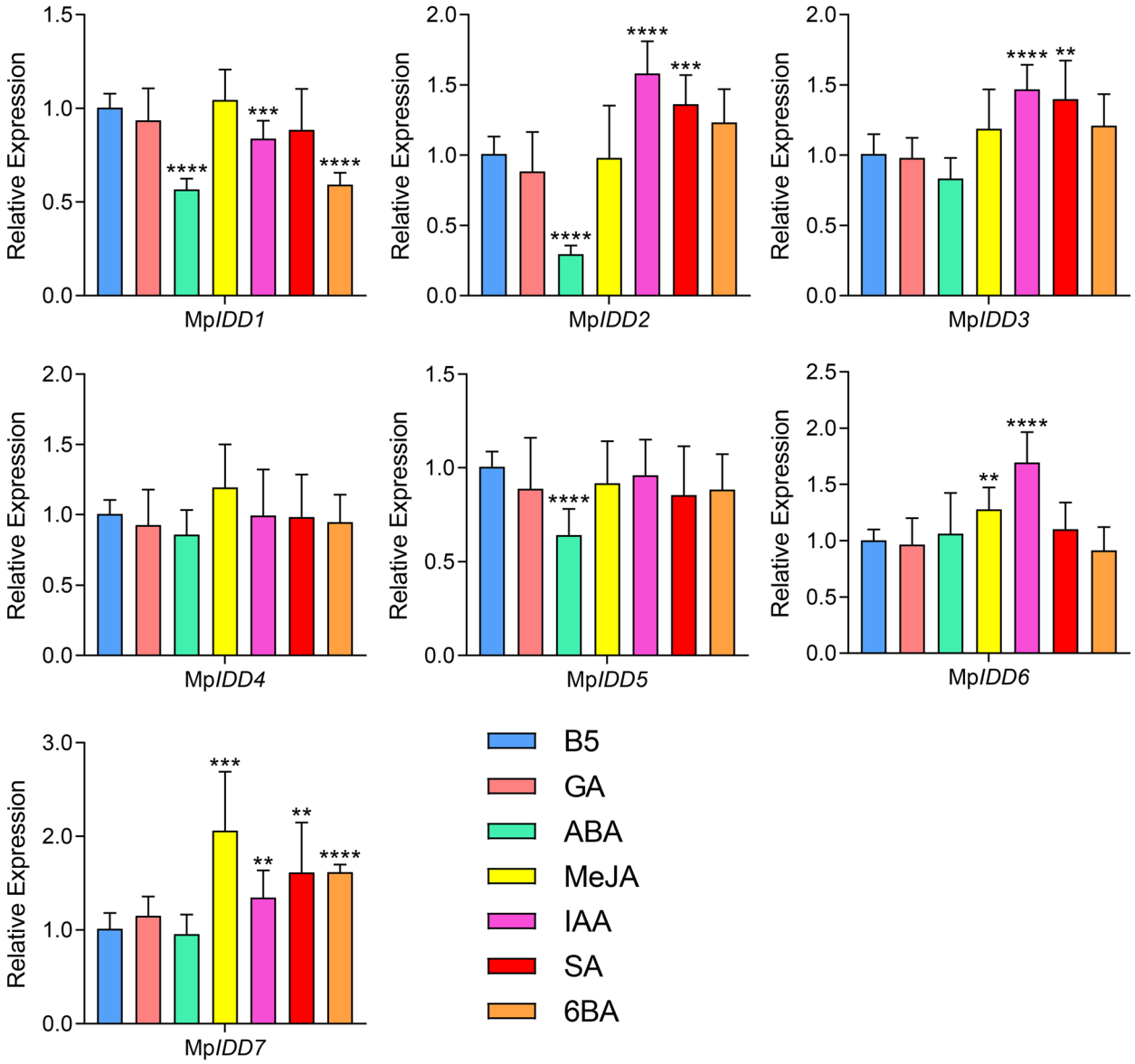

Fig. 6 Mp*IDD*s relative expression level under different plant hormone treatments. Transcript levels were determined in whole sample by qRT-PCR under hormones stresses. The bars are means ± standard deviation (SD) from three biological replicates and three technical replicates; Three biological replicates were presented in Fig. S4. *t*- tests, ** $P < 0.01$; *** $P < 0.001$; **** $P < 0.0001$. Mp*EF1α* was used as an internal control and the expression levels of Mp*IDD*s on 1/2 B5 medium were set to 1

then transformed into yeast strain AH109. The growth conditions and the blue color of the colonies on the histidine-deficient plates were monitored to assess the transcriptional activation activity of MpIDDs (Fig. 8). The result showed that all the yeast cells grew normally on the SD:/-Trp plate, suggesting the successful transformation of the recombinants (Fig. 8, the left three columns). The cells carrying pGBKT7-Mp*IDD1*, pGBKT7-Mp*IDD4* and pGBKT7-Mp*IDD5* grew well on the SD:/-Trp,-His plate, and displayed dark blue on SD:/-Trp,-His + X-α-gal plate (Fig. 8, the 1st, 4th and 5th rows), but the negative control (pGBKT7) failed to grow on the histidine-deficient plates (Fig. 8, the last row). suggesting the strong autoactivation activity of these three proteins. The cells carrying pGBKT7-Mp*IDD2* and pGBKT7-Mp*IDD3* grew moderately on the SD:/-Trp,-His plate, and displayed light blue on SD:/-Trp,-His + X-α-gal plates (Fig. 8, the 2nd and 3rd rows), indicating that these two proteins had weak autoactivation activity. The cells carrying pGBKT7-Mp*IDD6* and pGBKT7-Mp*IDD7* did not grow on the

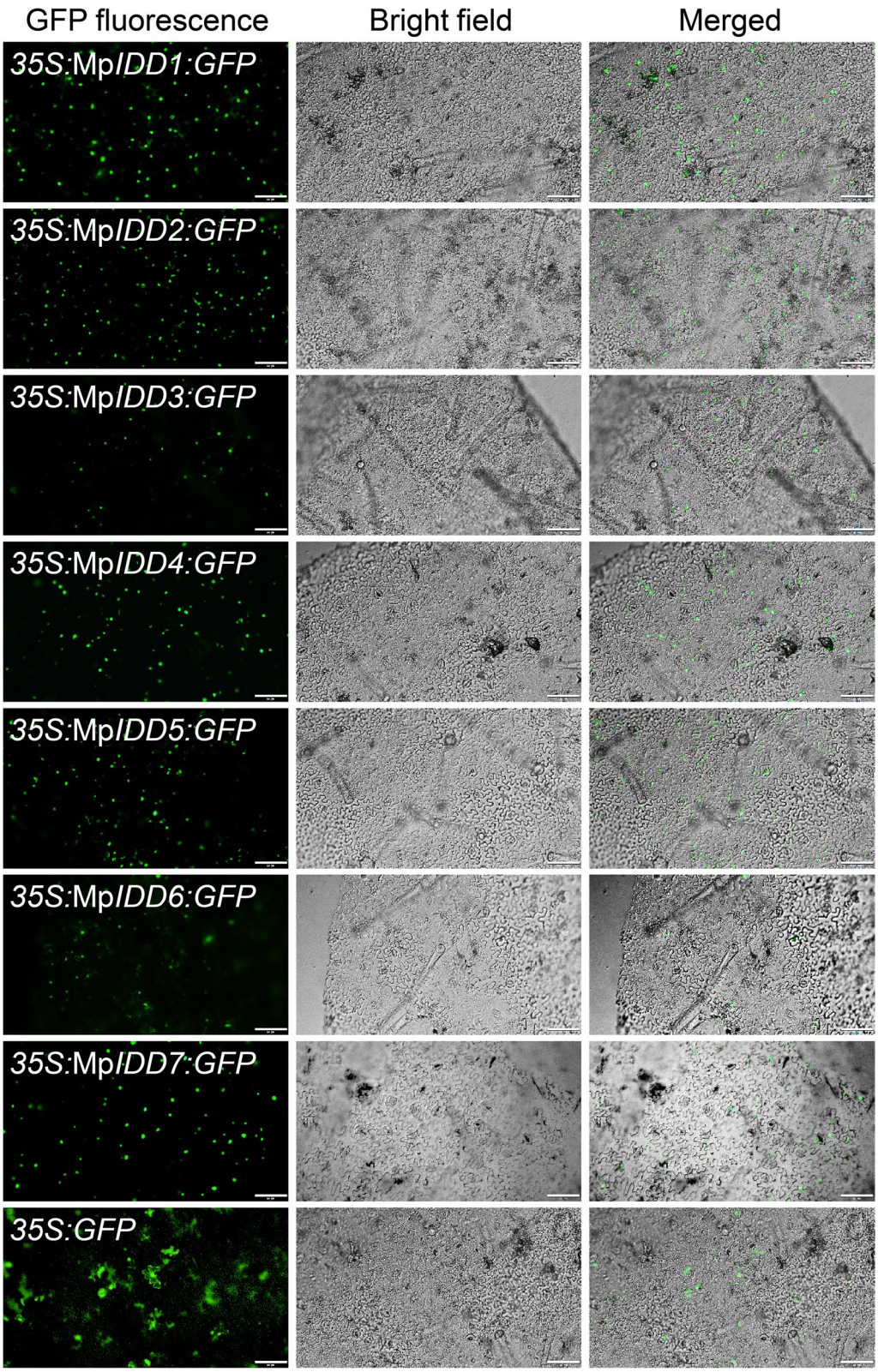

Fig. 7 Subcellular localization assay of MpIDDs. The transient expression of the *35S*:Mp*IDDs*:*Green fluorescent protein* (*GFP*) fusing constructs and *35S*:*GFP* construct in *Nicotiana tabacum* were performed. GFP signals were observed using an Olympus BX53F compound microscope. Scale bar = 100 μm

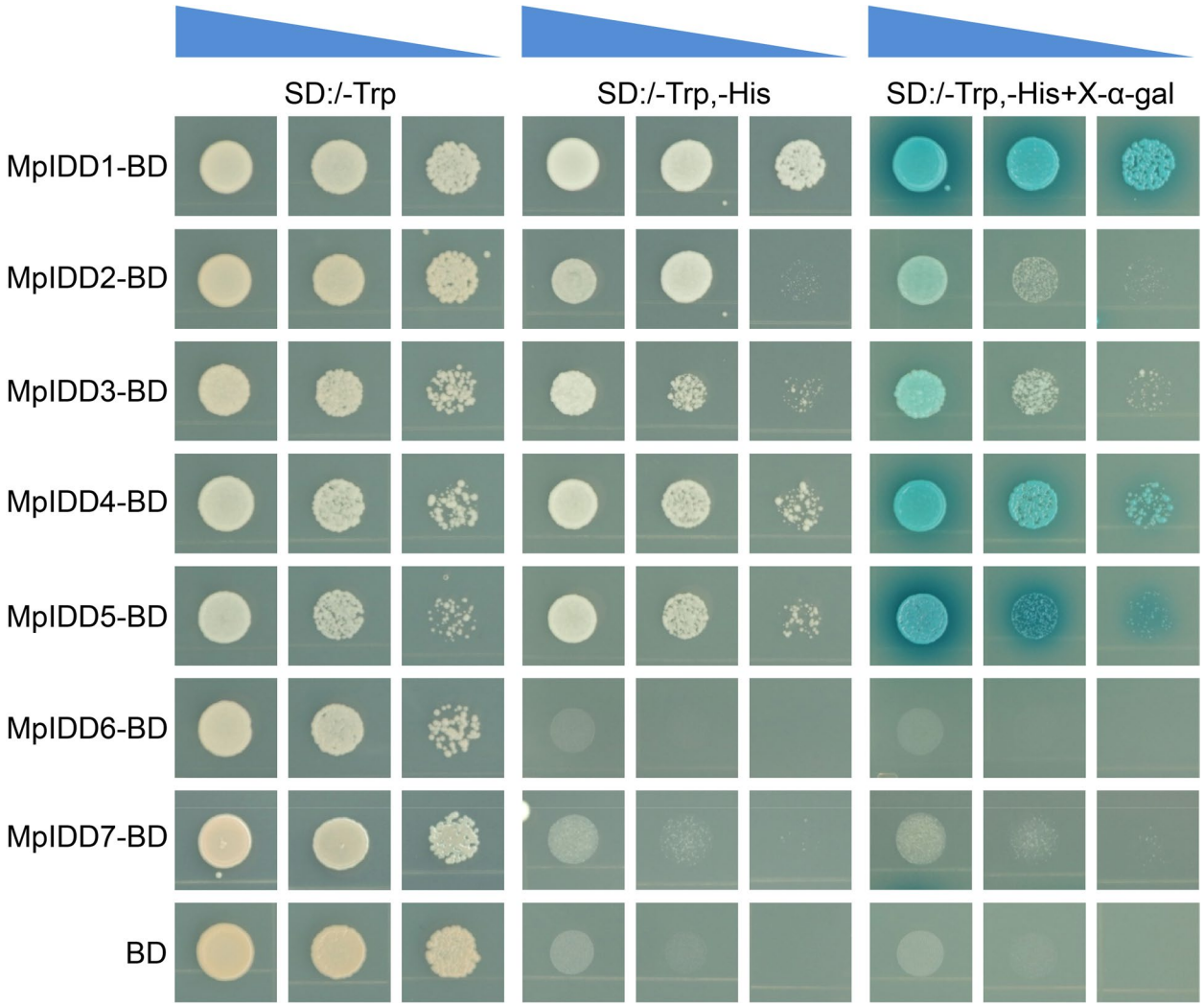

Fig. 8 Autoactivation assay of MpIDDs. The transformed yeast cells were first cultured on SD:/-Trp medium and then selected both on SD:/-Trp,-His and SD:/-Trp,-His + X-α-gal medium. The pGBKT7 vector was used as a negative control

histidine-deficient plates (Fig. 8, the 6th and 7th rows), suggesting lack of autoactivation activity in MpIDD6 and MpIDD7.

The interactions between MpIDDs and MpGRAS8/MpSHR or MpGRAS3/MpSCR

To search for the orthologs of AtSHR and AtSCR in *M. polymorpha* genome, a phylogenetic tree was constructed using the full-length deduced amino acid sequences of *GRAS* family proteins from *Arabidopsis* and *M. polymorpha* (Fig. S5). MpGRAS8 and AtSHR (support value 79) were obviously homologous based on interior-branch test analysis. Although the support value was low, MpGRAS3 was the closest GRAS protein in *M. polymorpha* to AtSCR (Fig. S5). A phylogenomic analysis from 19 taxa representing the major green lineages also provided evidence that MpGRAS3 with AtSCR, and MpGRAS8 with AtSHR share more homology [49]. The possible reason for the low support value of MpGRAS3 and AtSCR may be due to the distant relationship between the first land plant *M. polymorpha* and the angiosperm *Arabidopsis*.

We determined protein–protein interactions between the seven MpIDDs and MpGRAS8/MpSHR or MpGRAS3/MpSCR using yeast two-hybrid assay (Fig. 9). Five MpIDD members could interact with MpGRAS8/MpSHR or MpGRAS3/MpSCR. For MpGRAS8/MpSHR, MpIDD3 appeared to be the strongest interactor, while MpIDD4 and MpIDD5 interacted only weakly. Despite a strong autoactivation activity in the MpGRAS3/MpSCR-BD fusion protein, MpIDD1 and MpIDD2 clearly displayed stronger signals than the negative control. In summary, our results showed that most MpIDDs function together with MpGRAS8/MpSHR or MpGRAS3/MpSCR.

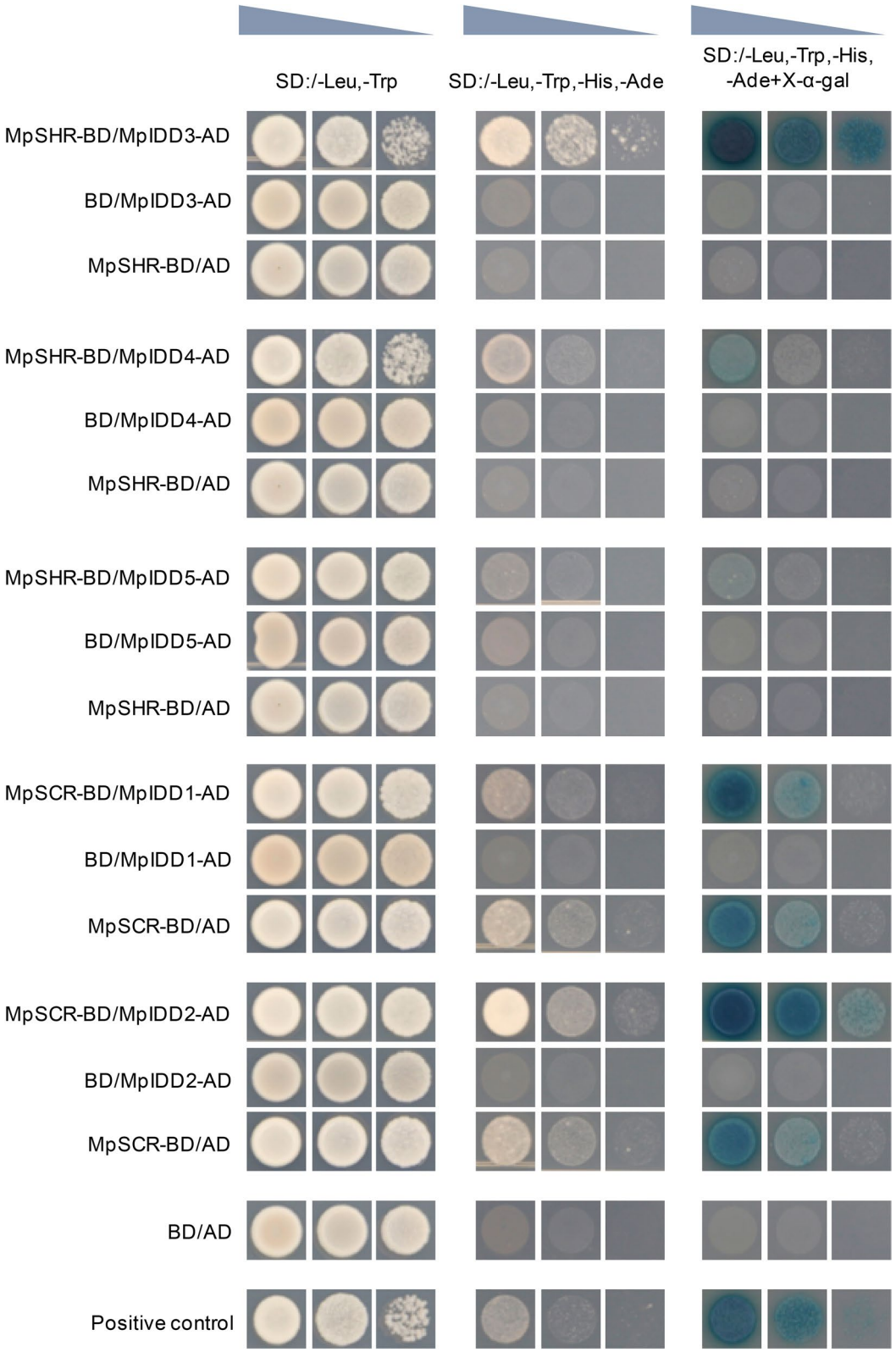

Fig. 9 Interactions of MpIDDs with MpGRAS8/MpSHR or MpGRAS3/MpSCR. Yeast cells transformed with different combinations of prey and bait plasmids were grown on the SD:/-Leu,-Trp, SD:/-Leu,-Trp,-His,-Ade as well as SD:/-Leu,-Trp,-His,-Ade + X-α-gal medium

Discussion

IDD gene family encodes plant-specific TFs that regulate various aspects of plant growth and development. Seven *IDD* genes are found in the genome of the liverwort *M. polymorpha* (Fig. 1) [29]. Thus far, only Mp*IDD6*/Mp*WIP* has been reported to have a role in controlling air pore complex formation [50]. The functions of most Mp*IDD*s await being revealed.

According to our phylogenetic tree, all the IDDs from 12 plant species can be divided into seven branches (I-VII, Fig. 1). In branch I, MpIDD3 shows relatively high homology to AtIDD3/MGP and AtIDD8/NUC, which participate in the SHR-SCR regulatory network to regulate ground tissue patterning in *Arabidopsis* root (Fig. 1) [6–8, 10]. We found the SHR binding motif in MpIDD3, and our yeast two-hybrid results suggest that MpGRAS8/MpSHR strongly interacts with MpIDD3 (Fig. 9). However, Mp*IDD3* does not show tissue specificity in the meristem, gemma cup, gemma or rhizoid, but displays a slightly higher expression level in the thallus (Fig. 5). Therefore, we infer that the MpSHR-MpIDD3 complex might play a part in the development of thallus. Additionally, AtIDD8 links the sugar signaling with photoperiodic flowering [51], and AtIDD3 was previously shown to bind to DELLA and respond to GA, a key determinant of floral transition in angiosperms [52, 53]. Nevertheless, our promoter element analysis failed to identify any GA responsive element in the 3.0 kb promoter of Mp*IDD3* (Fig. 4, Table S3), and only IAA and SA can elevate the expression level of Mp*IDD3* (Fig. 6). In our hormone treatment assay, none of the Mp*IDD*s responded to GA_3 (Fig. 6). GAs are a variety of tetracyclic diterpenoid compounds produced and sensed by many plants, especially by angiosperms. Sun et al. reported that only *ent*-kaurenoic acid (KA) and GA_{12}, two intermediates in GA biosynthesis pathway, could be synthesized by *M. polymorpha*, and many common forms of GAs, GA_1, GA_3 and GA_4, for instance, showed no bioactivity in the liverwort *M. polymorpha* [54]. For this reason, we could not rule out that the expression level of Mp*IDD3* might be changed by KA or GA_{12}. Further examination of the Mp*IDD3* expression pattern and function in sexual organs is required to define the role of Mp*IDD3* in sexual reproduction.

In branch III, MpIDD7, ZmID1 and OsID1 share high sequence similarities (Fig. 1). *ZmID1* and *OsID1*, mainly expressed in leaves, regulate the expression of flowering-time genes in the transition from vegetative growth to flowering [55–60]. Our tissue expression data concerning the vegetative growth phase identified a high expression level of Mp*IDD7* in gemma-cup and meristem (Fig. 5). From Marpolbase Expression Database (https://mbex.marchantia.info/), we found that the transcription level of Mp*IDD7* is high in the sexual organs in *M. polymorpha*. It can be deduced that Mp*IDD7* has broader expression than its counterparts in rice and maize and may also promote flowering in early land plant through a similar pathway. Besides, the expression of Mp*IDD7* can be elevated remarkably by MeJA and cytokinin treatments (Fig. 6). Exogenous MeJA treatments can induce genes involved in flower developments in oilseed rape and promote the opening of sorghum florets [61, 62]. Cytokinin promotes flowering in *Arabidopsis* but suppresses flowering in rice and maize [63, 64]. By mediating crosstalk between MeJA and cytokinin pathways, MpIDD7 might regulate flowering through an ancestral mechanism co-opted by angiosperms.

MpIDD2 belongs to branch IV, which consists of many regulators of auxin signaling in angiosperms. AtIDD14, AtIDD15 and AtIDD16 influence lateral organ morphogenesis and gravitropic responses by directly targeting genes in auxin biosynthesis and transport [25]. *OsIDD14*/*Loose Plant Architecture1* (*LPA1*) is highly expressed in the lamina joint, internodes, older tiller base and leaf sheath pulvinus, and affects the tiller angle, shoot gravitropism, lamina inclination and resistance to sheath blight disease via manipulating auxin flux [65–67]. The repression of the auxin transporter gene *OsPIN5c* by OsIDD12 and OsIDD13 is responsible for the SHR-mediated minor vein differentiation in rice [11]. In agreement with these, our results showed that Mp*IDD2* is greatly induced by IAA treatment (Fig. 6). Additionally, Mp*IDD2* has a gemma-cup specific expression pattern (Fig. 5). Gemma cup is an organ that is periodically produced on the dorsal midrib of the thallus in *M. polymorpha*, and gives birth to hundreds of gemmae as a means of vegetative reproduction [68]. Most IDDs from *Arabidopsis* and rice in this branch are concerned with lateral organ morphogenesis, such as branch orientation, tiller angle and lamina inclination [25, 65, 66]. A recent study supported the notion that the mechanisms for gemma cup generation in *M. polymorpha* and lateral organ formation in angiosperms are conserved [69]. Therefore, there is a high probability that MpIDD2 controls the gemma cup development via an auxin-dependent pathway. Remarkably, the *scr* mutant lacks endodermis in the inflorescence stem and shows horizontal lateral branches that is agravitropic [19, 70]. We discovered that MpGRAS3/MpSCR has an intense affinity to MpIDD2 (Fig. 9), implying that MpSCR-MpIDD2 complex is likely to be a key element in gemma cup establishment during early land plant evolution. Moreover, the expression level of Mp*IDD2* is significantly changed by ABA and SA treatment (Fig. 6), suggesting that Mp*IDD2* might respond to stresses.

Mp*IDD6*/Mp*WIP* is a member of branch VI. The promoter of Mp*IDD6*/Mp*WIP* is active in developing air pores, and its reduced expression causes air pore

complex defect [50]. Our result showed that Mp*IDD6*/Mp*WIP* is highly expressed in gemmae and meristem by means of tissue quantitative RT-PCR (Fig. 5), which does not have the resolution to tell if it is expressed in air pores. Further information we have provided is that Mp*IDD6*/Mp*WIP* is up-regulated by IAA or MeJA treatment (Fig. 6). In angiosperms, auxin level is negatively correlated with the number of stomata [71, 72]. JA signaling can trigger stomatal closure through activating K^+ channel by a Ca^{2+} sensor-kinase complex [73], and yet the air pore in the liverwort *M. polymorpha* cannot open and close as stomata [68]. Hence, it will be interesting to investigate whether auxin and JA signaling have a role in air pore development in the early land plants. Besides, it is noteworthy that, in rice and green millet, the orthologs of AtSHR or AtSCR all mediate stomatal patterning [11, 74–76]. Further mechanism study revealed a connection of OsSHRs with OsIDD12/OsIDD13 (the branch IV members) as well as auxin transport [11], which points to the possibility that Mp*IDD6*/Mp*WIP* mediated air pore development maybe auxin-related. Moreover, genetic analysis showed that MpIDD6/MpWIP might act as a transcriptional repressor [50], coinciding with our biochemical results that MpIDD6/MpWIP had no autoactivation activity (Fig. 8).

Although the remaining three MpIDDs are grouped with IDD proteins of unknown functions in the phylogenetic tree (Fig. 1), which gives us no further information, we attempted to interpret the functions of these three genes from other data. The transcript of Mp*IDD1* is abundant in meristem and downregulated by ABA, IAA or 6BA treatment, and MpIDD1 binds to MpGRAS3/MpSCR (Fig. 5, Fig. 6 and Fig. 9). Auxin and cytokinin act synergistically or antagonistically in shoot apical meristem formation and maintenance in angiosperms [77]. ABA can modulate the cell proliferation in the root meristem in *Arabidopsis* [78]. To be sure, further experiments are needed to verify the function of the MpSCR-MpIDD1 complex in meristem development in *M. polymorpha*. Once confirmed, it is proposed to investigate whether auxin, cytokinin or ABA signaling are involved in this process. MpIDD4 and MpIDD5 are also detected as MpGRAS8/MpSHR bound co-regulators, although the interactions are weak (Fig. 9). Unfortunately, no tissue-specificity or hormone treatment responsiveness concerning Mp*IDD4* could be deduced from our results. Mp*IDD5* displays an extremely high expression level in rhizoids (Fig. 5), and is repressed by ABA treatment (Fig. 6). It is believed that the rhizoids of bryophytes and root hairs of angiosperms are evolutionary conserved [79]. ROOTHAIR DEFECTIVE SIX-LIKE (RSL) transcription factor positively regulates rhizoids development in the angiosperm *Arabidopsis* and the bryophytes *P. patens* and *M. polymorpha* [80, 81]. ABA negatively controls root hair growth in *Arabidopsis* through OBF BINDING PROTEIN4 (OBP4)-mediated inhibition of *RSL2* [82]. In line with this view, it is worth exploring the function of the MpGRAS8/MpSHR-MpIDD5 complex in rhizoid formation in *M. polymorpha* and determining whether this process is regulated via a conserved ABA-dependent way.

Conclusions

In conclusion, we have identified the phylogenetic relationship between MpIDDs and IDDs in representative plants from different taxa. The Mp*IDD*s gene structures were analyzed to confirm the conserved gene organization of this family. Protein motif search showed the existence of classic C2H2 and noncanonical zinc fingers in MpIDDs, and protein structure prediction presented the core domain similarity between MpIDDs and related IDDs from the same phylogenetic groups. Tissue-specific expression pattern analysis revealed the Mp*IDD*s enriched in meristem, gemma cup, gemma and rhizoid respectively. Most Mp*IDD*s respond transcriptionally to at least one kind of hormone, in accordance with the presence of multiple *cis*-regulatory elements in their promoter sequences. All MpIDDs are nuclear localized and most have autoactivity. Results from yeast two-hybrid assays raised the possibility that the MpIDDs also act as co-transcription factors of MpGRAS8/MpSHR or MpGRAS3/MpSCR, resembling the situation in angiosperms. Our results thus provide valuable information for further elucidating Mp*IDD*s gene functions.

Supplementary Information

The online version contains supplementary material available at https://doi.org/10.1186/s12864-025-11609-7.

Supplementary Material 1.

Supplementary Material 2.

Supplementary Material 3.

Supplementary Material 4.

Supplementary Material 5.

Supplementary Material 6.

Supplementary Material 7: Fig. S1 The consensus sequences of conserved motifs in MpIDD gene family. Fig. S2 The reliability of the predicted IDD structures. Blue, cyan, yellow and orange represented confidence > 90%, 70-90%, 50-70% and < 50%, respectively. Fig. S3 The expression level of MpIDD1 to 7 in different tissues of three-week-old M. polymorpha. A. The second biological replicate. B. The third biological replicate. Fig. S4 MpIDDs relative expression level under phytohormone treatments. A. The first biological replicate. B. The second biological replicate. C. The third biological replicate. Fig. S5 Phylogenetic tree showing evolutionary relationships of GRAS family proteins in Arabidopsis and M. polymorpha. The evolutionary history was inferred by using the Maximum Likelihood method based on the Poisson correction model [83]. The tree with the highest log likelihood (-29597.43) is shown. The percentage of trees in which the associated taxa clustered together is shown next to the branches. Initial tree(s) for

the heuristic search were obtained automatically by applying Neighbor-Join and BioNJ algorithms to a matrix of pairwise distances estimated using a JTT model, and then selecting the topology with superior log likelihood value. The tree is drawn to scale, with branch lengths measured in the number of substitutions per site. The analysis involved 46 amino acid sequences obtained from Phytozome (Marchantia polymorpha v6.1, Arabidopsis thaliana TAIR10) and the accession numbers of GRAS genes were listed in Table S1. All positions with less than 80% site coverage were eliminated. That is, fewer than 20% alignment gaps, missing data, and ambiguous bases were allowed at any position. There was a total of 358 positions in the final dataset. Evolutionary analyses were conducted in MEGA7 [84].

Acknowledgements
We thank Dr. Chizuko Yamamuro (Fujian Agriculture and Forestry University, China) for providing the Tak-1 material.

Authors' contributions
C.Y.Z., J.F. and M.L.C. conducted the experiments; T.Y. provided technical assistance; H.C.C. edited the manuscript and provided advice; F.Y. supervised C.Y.Z.; H.W.L.supervised M.L.C.; J.F. wrote the manuscript. All authors read and approved the manuscript.

Funding
This work was supported by a grant from the Northwest A&F University (K5020223594).

Data availability
Data is provided within the manuscript or supplementary information files.

Declarations

Ethics approval and consent to participate
Not applicable.

Consent for publication
Not applicable.

Competing interests
The authors declare no competing interests.

Author details
[1]State Key Laboratory of Crop Stress Biology for Arid Areas and College of Life Sciences, Northwest A&F University, Yangling, Shaanxi 712100, China. [2]Department of Biological Science, Florida State University, Tallahassee, FL 32306, USA.

Received: 28 August 2024 Accepted: 17 April 2025
Published online: 29 April 2025

References

1. Helariutta Y, Fukaki H, Wysocka-Diller J, Nakajima K, Jung J, Sena G, Hauser MT, Benfey PN. The *SHORT-ROOT* gene controls radial patterning of the *Arabidopsis* root through radial signaling. Cell. 2000;101(5):555–67.
2. Di Laurenzio L, Wysocka-Diller J, Malamy JE, Pysh L, Helariutta Y, Freshour G, Hahn MG, Feldmann KA, Benfey PN. The *SCARECROW* gene regulates an asymmetric cell division that is essential for generating the radial organization of the *Arabidopsis* root. Cell. 1996;86(3):423–33.
3. Benfey PN, Linstead PJ, Roberts K, Schiefelbein JW, Hauser MT, Aeschbacher RA. Root development in *Arabidopsis*: four mutants with dramatically altered root morphogenesis. Development. 1993;119(1):57–70.
4. Cui H, Kong D, Liu X, Hao Y. SCARECROW, SCR-LIKE 23 and SHORT-ROOT control bundle sheath cell fate and function in *Arabidopsis thaliana*. Plant J. 2014;78(2):319–27.
5. Yoon EK, Dhar S, Lee MH, Song JH, Lee SA, Kim G, Jang S, Choi JW, Choe JE, Kim JH, Lee MM, Lim J. Conservation and Diversification of the SHR-SCR-SCL23 Regulatory Network in the Development of the Functional Endodermis in *Arabidopsis* Shoots. Mol Plant. 2016;9(8):1197–209.
6. Levesque MP, Vernoux T, Busch W, Cui H, Wang JY, Blilou I, Hassan H, Nakajima K, Matsumoto N, Lohmann JU, Scheres B, Benfey PN. Whole-genome analysis of the SHORT-ROOT developmental pathway in *Arabidopsis*. PLoS Biol. 2006;4(5):e143.
7. Cui H, Levesque MP, Vernoux T, Jung JW, Paquette AJ, Gallagher KL, Wang JY, Blilou I, Scheres B, Benfey PN. An evolutionarily conserved mechanism delimiting SHR movement defines a single layer of endodermis in plants. Science. 2007;316(5823):421–5.
8. Welch D, Hassan H, Blilou I, Immink R, Heidstra R, Scheres B. *Arabidopsis* JACKDAW and MAGPIE zinc finger proteins delimit asymmetric cell division and stabilize tissue boundaries by restricting SHORT-ROOT action. Genes Dev. 2007;21(17):2196–204.
9. Long Y, Smet W, Cruz-Ramírez A, Castelijns B, de Jonge W, Mähönen AP, Bouchet BP, Perez GS, Akhmanova A, Scheres B, Blilou I. *Arabidopsis* BIRD Zinc Finger Proteins Jointly Stabilize Tissue Boundaries by Confining the Cell Fate Regulator SHORT-ROOT and Contributing to Fate Specification. Plant Cell. 2015;27(4):1185–99.
10. Moreno-Risueno MA, Sozzani R, Yardımcı GG, Petricka JJ, Vernoux T, Blilou I, Alonso J, Winter CM, Ohler U, Scheres B, Benfey PN. Transcriptional control of tissue formation throughout root development. Science. 2015;350(6259):426–30.
11. Liu Q, Teng S, Deng C, Wu S, Li H, Wang Y, Wu J, Cui X, Zhang Z, Quick WP, Brutnell TP, Sun X, Lu T, Liu Q. SHORT ROOT and INDETERMINATE DOMAIN family members govern *PIN-FORMED* expression to regulate minor vein differentiation in rice. Plant Cell. 2023;35(8):2848–70.
12. Sozzani R, Cui H, Moreno-Risueno MA, Busch W, Van Norman JM, Vernoux T, Brady SM, Dewitte W, Murray JL, Benfey PN. Spatiotemporal regulation of cell-cycle genes by SHORTROOT links patterning and growth. Nature. 2010;466(7302):128–32.
13. Cruz-Ramírez A, Diaz-Trivino S, Blilou I, Grieneisen VA, Sozzani R, Zamioudis C, Miskolczi P, Nieuwland J, Benjamins R, Dhonukshe P, Caballero-Pérez J, Horvath B, Long Y, Mähönen AP, Zhang H, Xu J, Murray JA, Benfey PN, Bakó L, Marée AF, Scheres B. A bistable circuit involving SCARECROW-RETINOBLASTOMA integrates cues to inform asymmetric stem cell division. Cell. 2012;150(5):1002–15.
14. Nakajima K, Sena G, Nawy T, Benfey PN. Intercellular movement of the putative transcription factor SHR in root patterning. Nature. 2001;413(6853):307–11.
15. Heidstra R, Welch D, Scheres B. Mosaic analyses using marked activation and deletion clones dissect *Arabidopsis* SCARECROW action in asymmetric cell division. Genes Dev. 2004;18(16):1964–9.
16. Wildwater M, Campilho A, Perez-Perez JM, Heidstra R, Blilou I, Korthout H, Chatterjee J, Mariconti L, Gruissem W, Scheres B. The *RETINOBLASTOMA-RELATED* gene regulates stem cell maintenance in *Arabidopsis* roots. Cell. 2005;123(7):1337–49.
17. Gardiner J, Donner TJ, Scarpella E. Simultaneous activation of *SHR* and *ATHB8* expression defines switch to preprocambial cell state in *Arabidopsis* leaf development. Dev Dyn. 2011;240(1):261–70.
18. Wysocka-Diller JW, Helariutta Y, Fukaki H, Malamy JE, Benfey PN. Molecular analysis of *SCARECROW* function reveals a radial patterning mechanism common to root and shoot. Development. 2000;127(3):595–603.
19. Fukaki H, Fujisawa H, Tasaka M. *SGR1*, *SGR2*, *SGR3*: novel genetic loci involved in shoot gravitropism in *Arabidopsis thaliana*. Plant Physiol. 1996;110(3):945–55.
20. Colasanti J, Tremblay R, Wong AY, Coneva V, Kozaki A, Mable BK. The maize *INDETERMINATE1* flowering time regulator defines a highly conserved zinc finger protein family in higher plants. BMC Genomics. 2006;7:158.
21. Coelho CP, Huang P, Lee DY, Brutnell TP. Making Roots, Shoots, and Seeds: *IDD* Gene Family Diversification in Plants. Trends Plant Sci. 2018;23(1):66–78.
22. Hirano Y, Nakagawa M, Suyama T, Murase K, Shirakawa M, Takayama S, Sun TP, Hakoshima T. Structure of the SHR-SCR heterodimer bound to the BIRD/IDD transcriptional factor JKD. Nat Plants. 2017;3:17010.
23. Deng L, Li L, Zhang S, Shen J, Li S, Hu S, Peng Q, Xiao J, Wu C. Suppressor of rid1 (SID1) shares common targets with RID1 on florigen genes to initiate floral transition in rice. PLoS Genet. 2017;13(2):e1006642.
24. Schnable PS, Ware D, Fulton RS, Stein JC, Wei F, Pasternak S, Liang C, Zhang J, Fulton L, Graves TA, Minx P, Reily AD, Courtney L, Kruchowski SS, Tomlinson C, Strong C, Delehaunty K, Fronick C, Courtney B, Rock SM,

Belter E, Du F, Kim K, Abbott RM, Cotton M, Levy A, Marchetto P, Ochoa K, Jackson SM, Gillam B, Chen W, Yan L, Higginbotham J, Cardenas M, Waligorski J, Applebaum E, Phelps L, Falcone J, Kanchi K, Thane T, Scimone A, Thane N, Henke J, Wang T, Ruppert J, Shah N, Rotter K, Hodges J, Ingenthron E, Cordes M, Kohlberg S, Sgro J, Delgado B, Mead K, Chinwalla A, Leonard S, Crouse K, Collura K, Kudrna D, Currie J, He R, Angelova A, Rajasekar S, Mueller T, Lomeli R, Scara G, Ko A, Delaney K, Wissotski M, Lopez G, Campos D, Braidotti M, Ashley E, Golser W, Kim H, Lee S, Lin J, Dujmic Z, Kim W, Talag J, Zuccolo A, Fan C, Sebastian A, Kramer M, Spiegel L, Nascimento L, Zutavern T, Miller B, Ambroise C, Muller S, Spooner W, Narechania A, Ren L, Wei S, Kumari S, Faga B, Levy MJ, McMahan L, Van Buren P, Vaughn MW, Ying K, Yeh CT, Emrich SJ, Jia Y, Kalyanaraman A, Hsia AP, Barbazuk WB, Baucom RS, Brutnell TP, Carpita NC, Chaparro C, Chia JM, Deragon JM, Estill JC, Fu Y, Jeddeloh JA, Han Y, Lee H, Li P, Lisch DR, Liu S, Liu Z, Nagel DH, McCann MC, SanMiguel P, Myers AM, Nettleton D, Nguyen J, Penning BW, Ponnala L, Schneider KL, Schwartz DC, Sharma A, Soderlund C, Springer NM, Sun Q, Wang H, Waterman M, Westerman R, Wolfgruber TK, Yang L, Yu Y, Zhang L, Zhou S, Zhu Q, Bennetzen JL, Dawe RK, Jiang J, Jiang N, Presting GG, Wessler SR, Aluru S, Martienssen RA, Clifton SW, McCombie WR, Wing RA, Wilson RK. The B73 maize genome: complexity, diversity, and dynamics. Science. 2009;326(5956):1112–5.

25. Cui D, Gregersen H, Jing Y, Fan M, Liu J, Wang Z, Xin W, Hu Y. The *Arabidopsis* IDD14, IDD15, and IDD16 cooperatively regulate lateral organ morphogenesis and gravitropism by promoting auxin biosynthesis and transport. PLoS Genet. 2013;9(9):e1003759.
26. Yi G, Neelakandan AK, Gontarek BC, Vollbrecht E, Becraft PW. The *naked endosperm* genes encode duplicate INDETERMINATE domain transcription factors required for maize endosperm cell patterning and differentiation. Plant Physiol. 2015;167(2):443–56.
27. Gontarek BC, Neelakandan AK, Wu H, Becraft PW. NKD Transcription Factors Are Central Regulators of Maize Endosperm Development. Plant Cell. 2016;28(12):2916–36.
28. Sun Q, Li DD, Chu J, Yuan P, Li S, Zhong LJ, Han X, Xuan YH. Indeterminate Domain Proteins Regulate Rice Defense to Sheath Blight Disease. Rice (N Y). 2020;13(1):15.
29. Bowman JL, Kohchi T, Yamato KT, Jenkins J, Shu S, Ishizaki K, Yamaoka S, Nishihama R, Nakamura Y, Berger F, Adam C, Aki S, Althoff F, Araki T, Arteaga-Vazquez MA, Balasubrmanian S, Barry K, Bauer D, Boehm CR, Briginshaw L, Caballero-Perez J, Catarino B, Chen F, Chiyoda S, Chovatia M, Davies KM, Delmans M, Demura T, Dierschke T, Dolan L, Dorantes-Acosta AE, Eklund DM, Florent SN, Flores-Sandoval E, Fujiyama A, Fukuzawa H, Galik B, Grimanelli D, Grimwood J, Grossniklaus U, Hamada T, Haseloff J, Hetherington AJ, Higo A, Hirakawa Y, Hundley HN, Ikeda Y, Inoue K, Inoue SI, Ishida S, Jia Q, Kakita M, Kanazawa T, Kawai Y, Kawashima T, Kennedy M, Kinose K, Kinoshita T, Kohara Y, Koide E, Komatsu K, Kopischke S, Kubo M, Kyozuka J, Lagercrantz U, Lin SS, Lindquist E, Lipzen AM, Lu CW, De Luna E, Martienssen RA, Minamino N, Mizutani M, Mizutani M, Mochizuki N, Monte I, Mosher R, Nagasaki H, Nakagami H, Naramoto S, Nishitani K, Ohtani M, Okamoto T, Okumura M, Phillips J, Pollak B, Reinders A, Rövekamp M, Sano R, Sawa S, Schmid MW, Shirakawa M, Solano R, Spunde A, Suetsugu N, Sugano S, Sugiyama A, Sun R, Suzuki Y, Takenaka M, Takezawa D, Tomogane H, Tsuzuki M, Ueda T, Umeda M, Ward JM, Watanabe Y, Yazaki K, Yokoyama R, Yoshitake Y, Yotsui I, Zachgo S, Schmutz J. Insights into Land Plant Evolution Garnered from the *Marchantia polymorpha* Genome. Cell. 2017;171(2):287-304.e15.
30. Ishizaki K, Nishihama R, Yamato KT, Kohchi T. Molecular Genetic Tools and Techniques for *Marchantia polymorpha* Research. Plant Cell Physiol. 2016;57(2):262–70.
31. Goodstein DM, Shu S, Howson R, Neupane R, Hayes RD, Fazo J, Mitros T, Dirks W, Hellsten U, Putnam N, Rokhsar DS. Phytozome: a comparative platform for green plant genomics. Nucleic Acids Res. 2012;40(Database issue):D1178–86.
32. Jin J, Tian F, Yang DC, Meng YQ, Kong L, Luo J, Gao G. PlantTFDB 4.0: toward a central hub for transcription factors and regulatory interactions in plants. Nucleic Acids Res. 2017;45(D1):D1040–5.
33. Larkin MA, Blackshields G, Brown NP, Chenna R, McGettigan PA, McWilliam H, Valentin F, Wallace IM, Wilm A, Lopez R, Thompson JD, Gibson TJ, Higgins DG. Clustal W and Clustal X version 2.0. Bioinformatics. 2007;23(21):2947–8.
34. Tamura K, Stecher G, Kumar S. Molecular Evolutionary Genetics Analysis Version 11. Mol Biol Evol. 2021;38(7):3022–7.
35. Liu W, Xie Y, Ma J, Luo X, Nie P, Zuo Z, Lahrmann U, Zhao Q, Zheng Y, Zhao Y, Xue Y, Ren J. IBS: an illustrator for the presentation and visualization of biological sequences. Bioinformatics. 2015;31(20):3359–61.
36. Bailey TL, Boden M, Buske FA, Frith M, Grant CE, Clementi L, Ren J, Li WW, Noble WS. MEME SUITE: tools for motif discovery and searching. Nucleic Acids Res. 2009;37(Web Server issue):W202–8.
37. Abramson J, Adler J, Dunger J, Evans R, Green T, Pritzel A, Ronneberger O, Willmore L, Ballard AJ, Bambrick J, Bodenstein SW, Evans DA, Hung CC, O'Neill M, Reiman D, Tunyasuvunakool K, Wu Z, Žemgulytė A, Arvaniti E, Beattie C, Bertolli O, Bridgland A, Cherepanov A, Congreve M, Cowen-Rivers AI, Cowie A, Figurnov M, Fuchs FB, Gladman H, Jain R, Khan YA, Low CMR, Perlin K, Potapenko A, Savy P, Singh S, Stecula A, Thillaisundaram A, Tong C, Yakneen S, Zhong ED, Zielinski M, Žídek A, Bapst V, Kohli P, Jaderberg M, Hassabis D, Jumper JM. Accurate structure prediction of biomolecular interactions with AlphaFold 3. Nature. 2024;630(8016):493–500.
38. Schrödinger L, DeLano W. 2020. PyMOL. Available at: http://www.pymol.org/pymol.
39. Lescot M, Déhais P, Thijs G, Marchal K, Moreau Y, Van de Peer Y, Rouzé P, Rombauts S. PlantCARE, a database of plant cis-acting regulatory elements and a portal to tools for *in silico* analysis of promoter sequences. Nucleic Acids Res. 2002;30(1):325–7.
40. Chen C, Chen H, Zhang Y, Thomas HR, Frank MH, He Y, Xia R. TBtools: An Integrative Toolkit Developed for Interactive Analyses of Big Biological Data. Mol Plant. 2020;13(8):1194–202.
41. Lewis LA, McCourt RM. Green algae and the origin of land plants. Am J Bot. 2004;91(10):1535–56.
42. Leliaert F, Smith DR, Moreau H, Herron MD, Verbruggen H, Delwiche CF, De Clerck O. Phylogeny and molecular evolution of the green algae. Crit Rev Plant Sci. 2012;31:1–46.
43. Rensing SA, Ick J, Fawcett JA, Lang D, Zimmer A, Van de Peer Y, Reski R. An ancient genome duplication contributed to the abundance of metabolic genes in the moss *Physcomitrella patens*. BMC Evol Biol. 2007;7:130.
44. Sagasser M, Lu GH, Hahlbrock K, Weisshaar BA. *thaliana* TRANSPARENT TESTA 1 is involved in seed coat development and defines the WIP subfamily of plant zinc finger proteins. Genes Dev. 2002;16(1):138–49.
45. Prochetto S, Reinheimer R. Step by step evolution of Indeterminate Domain (IDD) transcriptional regulators: from algae to angiosperms. Ann Bot. 2020;126(1):85–101.
46. Zhang T, Tan M, Geng L, Li J, Xiang Y, Zhang B, Zhao Y. New insight into comprehensive analysis of *INDETERMINATE DOMAIN* (*IDD*) gene family in rice. Plant Physiol Biochem. 2020;154:547–56.
47. Feng X, Yu Q, Zeng J, He X, Ma W, Ge L, Liu W. Comprehensive Analysis of the *INDETERMINATE DOMAIN* (*IDD*) Gene Family and Their Response to Abiotic Stress in *Zea mays*. Int J Mol Sci. 2023;24(7):6185.
48. Negi S, Itazu M, Imanishi M, Nomura A, Sugiura Y. Creation and characteristics of unnatural CysHis(3)-type zinc finger protein. Biochem Biophys Res Commun. 2004;325(2):421–5.
49. Cheng S, Xian W, Fu Y, Marin B, Keller J, Wu T, Sun W, Li X, Xu Y, Zhang Y, Wittek S, Reder T, Günther G, Gontcharov A, Wang S, Li L, Liu X, Wang J, Yang H, Xu X. Genomes of Subaerial *Zygnematophyceae* Provide Insights into Land Plant Evolution. Cell. 2019;179(5):1057-1067.e14.
50. Jones VA, Dolan L. Mp*WIP* regulates air pore complex development in the liverwort *Marchantia polymorpha*. Development. 2017;144(8):1472–6.
51. Seo PJ, Ryu J, Kang SK, Park CM. Modulation of sugar metabolism by an INDETERMINATE DOMAIN transcription factor contributes to photoperiodic flowering in *Arabidopsis*. Plant J. 2011;65(3):418–29.
52. Yoshida H, Hirano K, Sato T, Mitsuda N, Nomoto M, Maeo K, Koketsu E, Mitani R, Kawamura M, Ishiguro S, Tada Y, Ohme-Takagi M, Matsuoka M, Ueguchi-Tanaka M, et al. DELLA protein functions as a transcriptional activator through the DNA binding of the indeterminate domain family proteins. Proc Natl Acad Sci U S A. 2014;111(21):7861–6.
53. Bao S, Hua C, Shen L, Yu H. New insights into gibberellin signaling in regulating flowering in *Arabidopsis*. J Integr Plant Biol. 2020;62(1):118–31.
54. Sun R, Okabe M, Miyazaki S, Ishida T, Mashiguchi K, Inoue K, Yoshitake Y, Yamaoka S, Nishihama R, Kawaide H, Nakajima M, Yamaguchi S, Kohchi T. Biosynthesis of gibberellin-related compounds modulates far-red light responses in the liverwort *Marchantia polymorpha*. Plant Cell. 2023;35(11):4111–32.
55. Coneva V, Zhu T, Colasanti J. Expression differences between normal and indeterminate1 maize suggest downstream targets of ID1, a floral transition regulator in maize. J Exp Bot. 2007;58(13):3679–93.

56. Coneva V, Guevara D, Rothstein SJ, Colasanti J. Transcript and metabolite signature of maize source leaves suggests a link between transitory starch to sucrose balance and the autonomous floral transition. J Exp Bot. 2012;63(14):5079–92.
57. Meng X, Muszynski MG, Danilevskaya ON. The *FT-like ZCN8* Gene Functions as a Floral Activator and Is Involved in Photoperiod Sensitivity in Maize. Plant Cell. 2011;23(3):942–60.
58. Matsubara K, Yamanouchi U, Wang ZX, Minobe Y, Izawa T, Yano M. *Ehd2*, a rice ortholog of the maize *INDETERMINATE1* gene, promotes flowering by up-regulating *Ehd1*. Plant Physiol. 2008;148(3):1425–35.
59. Park SJ, Kim SL, Lee S, Je BI, Piao HL, Park SH, Kim CM, Ryu CH, Park SH, Xuan YH, Colasanti J, An G, Han CD. Rice *Indeterminate 1* (*Osid1*) is necessary for the expression of *Ehd1* (*Early heading date 1*) regardless of photoperiod. Plant J. 2008;56(6):1018–29.
60. Wu C, You C, Li C, Long T, Chen G, Byrne ME, Zhang Q. *RID1*, encoding a Cys2/His2-type zinc finger transcription factor, acts as a master switch from vegetative to floral development in rice. Proc Natl Acad Sci U S A. 2008;105(35):12915–20.
61. Pak H, Guo Y, Chen M, Chen K, Li Y, Hua S, Shamsi I, Meng H, Shi C, Jiang L. The effect of exogenous methyl jasmonate on the flowering time, floral organ morphology, and transcript levels of a group of genes implicated in the development of oilseed rape flowers (Brassica napus L.). Planta. 2009;231(1):79–91.
62. Liu S, Fu Y, He Y, Zeng X. Transcriptome analysis of the impact of exogenous methyl jasmonate on the opening of sorghum florets. PLoS ONE. 2021;16(3):e0248962.
63. D'Aloia M, Bonhomme D, Bouché F, Tamseddak K, Ormenese S, Torti S, Coupland G, Périlleux C. Cytokinin promotes flowering of *Arabidopsis* via transcriptional activation of the *FT* paralogue *TSF*. Plant J. 2011;65(6):972–9.
64. Cho LH, Yoon J, Tun W, Baek G, Peng X, Hong WJ, Mori IC, Hojo Y, Matsuura T, Kim SR, Kim ST, Kwon SW, Jung KH, Jeon JS, An G. Cytokinin increases vegetative growth period by suppressing florigen expression in rice and maize. Plant J. 2022;110(6):1619–35.
65. Wu X, Tang D, Li M, Wang K, Cheng Z. Plant Architecture1, an INDETERMINATE DOMAIN protein involved in shoot gravitropism, regulates plant architecture in rice. Plant Physiol. 2013;161(1):317–29.
66. Liu JM, Park SJ, Huang J, Lee EJ, Xuan YH, Je BI, Kumar V, Priatama RA, Raj KV, Kim SH, Min MK, Cho JH, Kim TH, Chandran AK, Jung KH, Takatsuto S, Fujioka S, Han CD. *Loose Plant Architecture1* (*LPA1*) determines lamina joint bending by suppressing auxin signalling that interacts with C-22-hydroxylated and 6-deoxo brassinosteroids in rice. J Exp Bot. 2016;67(6):1883–95.
67. Sun Q, Li TY, Li DD, Wang ZY, Li S, Li DP, Han X, Liu JM, Xuan YH. Overexpression of *Loose Plant Architecture 1* increases planting density and resistance to sheath blight disease via activation of *PIN-FORMED 1a* in rice. Plant Biotechnol J. 2019;17(5):855–7.
68. Shimamura M. *Marchantia polymorpha*: Taxonomy, Phylogeny and Morphology of a Model System. Plant Cell Physiol. 2016;57(2):230–56.
69. Yasui Y, Tsukamoto S, Sugaya T, Nishihama R, Wang Q, Kato H, Yamato KT, Fukaki H, Mimura T, Kubo H, Theres K, Kohchi T, Ishizaki K. GEMMA CUP-ASSOCIATED MYB1, an Ortholog of Axillary Meristem Regulators, Is Essential in Vegetative Reproduction in *Marchantia polymorpha*. Curr Biol. 2019;29(23):3987-3995.e5.
70. Kawamoto N, Kanbe Y, Nakamura M, Mori A, Terao MM. Gravity-Sensing Tissues for Gravitropism Are Required for "Anti-Gravitropic" Phenotypes of *Lzy* Multiple Mutants in *Arabidopsis*. Plants (Basel). 2020;9(5):615.
71. Balcerowicz M, Ranjan A, Rupprecht L, Fiene G, Hoecker U. Auxin represses stomatal development in dark-grown seedlings via Aux/IAA proteins. Development. 2014;141(16):3165–76.
72. Zhang JY, He SB, Li L, Yang HQ. Auxin inhibits stomatal development through MONOPTEROS repression of a mobile peptide gene *STOMAGEN* in mesophyll. Proc Natl Acad Sci U S A. 2014;111(29):E3015–23.
73. Förster S, Schmidt LK, Kopic E, Anschütz U, Huang S, Schlücking K, Köster P, Waadt R, Larrieu A, Batistič O, Rodriguez PL, Grill E, Kudla J, Becker D. Wounding-Induced Stomatal Closure Requires Jasmonate-Mediated Activation of GORK K^+ Channels by a Ca^{2+} Sensor-Kinase CBL1-CIPK5 Complex. Dev Cell. 2019;48(1):87-99.e6.
74. Schuler ML, Sedelnikova OV, Walker BJ, Westhoff P, Langdale JA. SHORTROOT-Mediated Increase in Stomatal Density Has No Impact on Photosynthetic Efficiency. Plant Physiol. 2018;176(1):757–72.
75. Wu Z, Chen L, Yu Q, Zhou W, Gou X, Li J, Hou S. Multiple transcriptional factors control stomata development in rice. New Phytol. 2019;223(1):220–32.
76. Hughes TE, Langdale JA. SCARECROW is deployed in distinct contexts during rice and maize leaf development. Development. 2022;149(7):dev200410.
77. Su YH, Liu YB, Zhang XS. Auxin-cytokinin interaction regulates meristem development. Mol Plant. 2011;4(4):616–25.
78. Belda-Palazón B, Costa M, Beeckman T, Rolland F, Baena-González E. ABA represses TOR and root meristem activity through nuclear exit of the SnRK1 kinase [published correction appears in. Proc Natl Acad Sci U S A. 2022;119(40):e2215090119.
79. Rensing SA. Plant Evo-Devo: How Tip Growth Evolved. Curr Biol. 2016;26(23):R1228–30.
80. Menand B, Yi K, Jouannic S, Hoffmann L, Ryan E, Linstead P, Schaefer DG, Dolan L. An ancient mechanism controls the development of cells with a rooting function in land plants. Science. 2007;316(5830):1477–80.
81. Proust H, Honkanen S, Jones VA, Morieri G, Prescott H, Kelly S, Ishizaki K, Kohchi T, Dolan L. *RSL Class* I Genes Controlled the Development of Epidermal Structures in the Common Ancestor of Land Plants. Curr Biol. 2016;26(1):93–9.
82. Rymen B, Kawamura A, Schäfer S, Breuer C, Iwase A, Shibata M, Ikeda M, Mitsuda N, Koncz C, Ohme-Takagi M, Matsui M, Sugimoto K. ABA Suppresses Root Hair Growth via the OBP4 Transcriptional Regulator. Plant Physiol. 2017;173(3):1750–62.
83. Zuckerkandl E, Pauling L. Evolutionary divergence and convergence in proteins. In: Bryson V, Vogel HJ, editors. Evolving Genes and Proteins. Academic Press: New York; 1965. p. 97–166.
84. Kumar S, Stecher G, Tamura K. MEGA7: Molecular Evolutionary Genetics Analysis Version 7.0 for Bigger Datasets. Mol Biol Evol. 2016;33(7):1870–4.

Publisher's Note